For submission to JBIC.

Bipyrimidine Ruthenium(II) Arene Complexes: Structure, Reactivity and Cytotoxicity

Soledad Betanzos-Lara,[a,b] Olga Novakova,[c] Robert J. Deeth,[a] Ana M. Pizarro,[a] Guy J. Clarkson,[a] Barbora Liskova,[c] Viktor Brabec,[c] Peter J. Sadler[a] and Abraha Habtemariam[a]✉

[a]Department of Chemistry, University of Warwick, Coventry, UK CV4 7AL; [b]Current address: Departamento de Química Inorgánica, Facultad de Química, Universidad Nacional Autónoma de México (UNAM), Ciudad Universitaria, Coyoacán, México, D.F. 04510; [c]Institute of Biophysics, Academy of Sciences of the Czech Republic, v.v.i., Kralovopolska 135, CZ61265 Brno, Czech Republic

E-mail: A.Habtemariam@warwick.ac.uk

ABSTRACT. The synthesis and characterization of complexes [(η^6-arene)Ru(*N*,*N*′)X][PF_6] where arene is *para*-cymene (*p*-cym), biphenyl (bip), ethyl benzoate (etb), hexamethylbenzene (hmb), indane (ind), or 1,2,3,4-tetrahydronaphthalene (thn); *N*,*N*′ is 2,2'-bipyrimidine (bpm), and X is Cl, Br, or I are reported, including the X-ray crystal structures of [(η^6-*p*-cym)Ru(bpm)I][PF_6] (**3**), [(η^6-bip)Ru(bpm)Cl][PF_6] (**4**), [(η^6-bip)Ru(bpm)I][PF_6] (**6**), and [(η^6-etb)Ru(bpm)Cl][PF_6] (**7**). Complexes in which *N*,*N*′ is 1,10-phenanthroline (phen), 1,10-phenanthroline-5,6-dione (phendio), or 4,7-diphenyl-1,10-phenanthroline (bathophen) were studied for comparison. The Ru^{II} arene complexes undergo ligand exchange reactions in aqueous solution at 310 K; their half-lives for hydrolysis vary from 14 to 715 min. Density functional theory (DFT) calculations on [(η^6-*p*-cym)Ru(bpm)Cl][PF_6] (**1**), [(η^6-*p*-cym)Ru(bpm)Br][PF_6] (**2**) and **3**–**6** suggest that aquation occurs via an associative pathway and that the reaction is thermodynamically favorable when the leaving ligand is I > Br ≈ Cl. pK_a* values for the aqua adducts of the complexes range from 6.9 to 7.32. A binding preference for 9-ethylguanine (9-EtG) compared to 9-ethyladenine (9-EtA) was observed for **1**, [(η^6-hmb)Ru(bpm)Cl]$^+$ (**8**), [(η^6-ind)Ru(bpm)Cl]$^+$ (**9**), [(η^6-thn)Ru(bpm)Cl]$^+$ (**10**), [(η^6-*p*-cym)Ru(phen)Cl]$^+$ (**11**) and [(η^6-*p*-cym)Ru(bathophen)Cl]$^+$ (**13**) in aqueous solution at 310 K. The X-ray crystal structure of the guanine complex [(η^6-*p*-cym)Ru(bpm)(9-EtG-*N7*)][PF_6]$_2$ (**14**) shows multiple H-bonding. DFT calculations show that the 9-EtG adducts of all complexes are thermodynamically preferred compared to those of 9-EtA. However, the bmp complexes are inactive towards A2780 human ovarian cancer-cells. Calf-thymus (CT)-DNA interactions for **1** and **11** consist of weak coordinative, intercalative, and monofunctional

coordination. Binding to biomolecules such as glutathione (GSH) may play a role in deactivating the bpm complexes.

Key Words

Ruthenium, arene, bipyrimidine, hydrolysis, nucleobase, DNA.

Introduction

The well-established mechanism of action of the cytotoxic drug cisplatin is the alteration of the secondary structure of DNA *via* coordination to the *N7* atom of a guanine (G) or an adenine (A) base, which requires its prior aquation in the cell to generate the more reactive aqua complexes $[Pt(NH_3)_2(OH_2)Cl]^+$ and $[Pt(NH_3)_2(OH_2)_2]^{2+}$ [1, 2]. In general, aquation can be an important activation step for transition metal complexes prior to their coordination to biomolecules [3]. Certain organometallic Ru^{II} complexes of the type $[(\eta^6\text{-arene})Ru(XY)Z]^{n+}$ where XY is a bidentate chelating ligand and Z is a leaving group, exhibit promising cytotoxic activity against a variety of cancer cell lines, including cisplatin-resistant cells [4, 5]. The nature of the arene, the chelating ligand, and the leaving group can have a major influence on the rates of activation (towards hydrolysis and/or binding to biomolecules) as well as on the cytotoxic activity [6]. It appears that the presence of a more hydrophobic arene ligand along with a single ligand exchange site is often associated with significant anticancer activity. Blocking ligand exchange reactions in the remaining two coordination sites can usually be achieved by coordination of a stable bidentate ligand; in this regard, particularly effective are those containing *N,N′*-heterocyclic groups [7, 8, 9].

In the present work, we have studied and contrasted the chemical reactivity of a series of organometallic Ru^{II} complexes of the type $[(\eta^6\text{-arene})Ru(N,N')X][PF_6]$ containing a *N,N′*-chelating ligand, as well as various arenes, and different halides (X). Their aqueous solution chemistry as well as the nucleobase binding (to 9-EtG and 9-EtA) were investigated. Their potential as cytotoxic agents was explored not only by determining IC_{50} values against A2780 (human ovarian), A2780cis (human ovarian cisplatin resistant), A549 (human lung) or HCT116 (human colon) cancer cell lines but also by studying DNA interactions in cell-free media. γ-Glutamyl-cysteinyl-glycine (glutathione, GSH) coordination to Pt(II) is known to inhibit DNA binding contributing to cisplatin resistance in tumor cells [10] and depending on its relative concentration [11, 12], it can both facilitate and/or inhibit ruthenium interactions with DNA [13]. Reactions of GSH with a representative inactive Ru^{II} arene complex (**1**) in aqueous solution at 310 K were therefore investigated in order to establish whether GSH may play a role in the activity of this family of complexes.

Materials and Methods

Materials. $RuCl_3 \cdot 3H_2O$ was acquired from Precious Metals Online (PMO Pty Ltd) and used as received. 2,2'-bipyrimidine (bpm), 1,10-phenanthroline (phen), 1,10-phenanthroline-5,6-dione (phendio), 4,7-diphenyl-1,10-phenanthroline (bathophen), 9-ethylguanine (9-EtG), 9-ethyladenine (9-EtA), and KPF_6 were obtained from Sigma-Aldrich. KBr and KI (reagent grade) were obtained from Fisher. The Ru^{II} arene precursor dimers $[(\eta^6\text{-arene})RuX_2]_2$ where arene is *para*-cymene (*p*-cym), biphenyl (bip), hexamethylbenzene (hmb), indane (ind), or tetrahydronaphthalene (thn) and X is Cl, Br, or I were synthesized according to a previously reported method [14]. The dimer $[(\eta^6\text{-etb})RuCl_2]_2$ where etb is ethylbenzoate was synthesized following published literature [15]. The solvents used for UV-vis absorption spectroscopy were dry methanol (reagent grade) and deionized water. For NMR spectroscopy, the solvents used were acetone-d_6, DMSO-d_6, methanol-d_4 and D_2O obtained from Aldrich. All chemicals were used without further purification. Cisplatin was obtained from Sigma-Aldrich (Prague, Czech Republic). Chloridodiethylenetriamineplatinum(II) chloride ([PtCl(dien)]Cl) was a generous gift of Professor Giovanni Natile from the University of Bari. Restriction endonucleases *Nde*I and *Hpa*I were purchased from New England Biolabs. Acrylamide, bis(acrylamide), and ethidium bromide (EtBr) were obtained from Merck KgaA (Darmstadt, Germany). Agarose was purchased from FMC BioProducts (Rockland, ME). Radioactive reagents were obtained from Amersham (Arlington Heights, IL, U.S.A.). Stock aqueous solutions of metal complexes (5×10^{-4} M) for the biophysical and biochemical studies were filtered and stored at room temperature in the dark. The concentrations of ruthenium or platinum in the stock solutions were determined by flameless atomic absorption spectrometry (FAAS). Calf

thymus CT-DNA (42% G + C, mean molecular mass ca. 2×10^7) was also prepared and characterized as described previously [16, 17]. pSP73KB (2455 bp) plasmid was isolated according to standard procedures [23].

Synthesis of Ruthenium Complexes. Complexes [(η^6-arene)Ru(*N,N′*)X][PF_6] where arene is *p*-cym, bip, etb, ind, hmb, or thn; *N,N′* is bpm, phen, phendio, or bathophen; and X is Cl, Br, or I were synthesized as previously described [6]. Typically, two mol equiv of the *N,N′* chelating ligand and two mol equiv of KPF_6 were added to a solution of one mol equiv of the appropriate Ru^{II} arene dimer in of dry methanol (20 mL) with constant stirring over 48 h upon which the precipitate formed was collected by filtration. The remaining solution was concentrated and portions of Et_2O were added to further precipitate the product which was again collected by filtration. Both solids were combined and washed with portions of Et_2O and MeOH and dried overnight under vacuum resulting in microcrystalline products. Details of the amounts of reactants, volumes of solvents, color changes, and nature of the products are described in the supporting information for the individual reactions, as well as any variations in the synthetic procedure. Some complexes were also characterized by ^{13}C NMR spectroscopy.

X-ray Crystallography. Diffraction data were collected either on an Oxford Diffraction Gemini four-circle system with a Ruby CCD area detector or on a Siemens SMART three-circle system with CCD area detector equipped with an Oxford Cryosystem Cooler. All structures were refined by full-matrix least squares against F^2 using SHELXL 97 [18]. The structures of complexes **3**, **4**, **6**, **7** and **14** were solved by direct methods using SHELXS [19] (TREF) with additional light atoms found by Fourier methods. Hydrogen atoms were added at calculated positions and refined using a riding model with freely rotating methyl

groups. Anisotropic displacement parameters were used for all non-H atoms; H-atoms were given isotropic displacement parameters equal to 1.2 (or 1.5 for methyl hydrogen atoms) times the equivalent isotropic displacement parameter of the atom to which the H-atom is attached.

NMR Spectroscopy. ^{1}H and ^{13}C NMR spectra were acquired in 5 mm NMR tubes at 298 K (unless otherwise stated) on either a Bruker AV-400, Bruker DRX-500, Bruker AV III 600 or Bruker AV II 700 NMR spectrometers. All data processing was carried out using XWIN-NMR version 3.6 (Bruker U.K. Ltd.). ^{1}H NMR chemical shifts were internally referenced to TMS *via* 1,4-dioxane (δ = 3.71) or residual MeOH (δ = 3.31). 1D spectra were recorded using standard pulse sequences. Typically, data were acquired with 128 transients into 16 k data points over a spectral width of 14 ppm. 2D COSY or TOCSY and NOESY spectra were recorded using standard pulse-pulse sequences. Typically, data were acquired with 72 transients into 1024 k data points over a spectral width of 14 ppm using a relaxation delay of 1.5 s and a mixing time of 0.06 s.

Elemental Analysis. Elemental analyses were performed by Exeter Analytical (U.K. Ltd.) using an CE-440 Elemental Analyzer.

High Resolution Electrospray Mass Spectrometry (HR-MS). HR-MS data were obtained on a Bruker MaXis UHR-TOF. All the samples were analyzed by positive-ion ESI(+) mass spectra. Samples were prepared either in 100% H_2O or 95% MeOH/5% H_2O mixture and typically injected at 2 μL min^{-1}, nebulizer gas (N_2) 0.4 bar, dry gas (N_2) 4 L min^{-1} and dry temp 453 K, Funnel RF 200V, Multiple RF 200, quadrupole ion energy 4 eV, collision cell 5 eV, ion cooler RF settings, ramp from 50 to 250 V, unless otherwise stated.

UV-vis Absorption Spectroscopy. UV-vis absorption spectra were recorded on a Cary 50-Bio spectrophotometer with a PTP1 Peltier temperature controller or on a Beckman DU 7400 UV-Vis spectrophotometer equipped with a thermoelectrically controlled cell holder, in a 1-cm pathlength quartz cells (600 μL). Spectra were recorded at 310 K in deionized water from 220 to 800 nm and were processed using UV-Winlab software for Windows 95 controller

pH* Measurement. pH values were measured at ambient temperature using a Corning 240 pH meter equipped with a micro combination KNO_3 (chloride free) electrode calibrated with Aldrich buffer solutions of pH 4, 7, and 10. The pH* values (pH meter reading without correction for effects of deuterium (D) on glass electrode) of NMR samples in D_2O were measured at about 298 K directly in the NMR tube, before and after recording NMR spectra, using the same method. The pH^* values were adjusted with dilute NaOH or HNO_3 solutions in D_2O.

pK_a* Values. For determinations of pK_a^* values (for solutions in D_2O), the pH^* values of solutions of the aqua complexes in D_2O were varied from *ca*. pH^* 1 to 12 by the addition of dilute NaOH or HNO_3 solutions in D_2O, and ^1H NMR spectra were recorded. The chemical shifts of the arene ring protons were plotted against pH^* values. The pH^* titration curves were fitted to the Henderson-Hasselbalch equation using ORIGIN version 8.0, with the assumption that the observed chemical shifts are weighted averages according to the populations of the protonated and deprotonated species. These pK_a^* values can be converted to pK_a values by use of the equation $pK_a = 0.929\ pK_a^* + 0.42$ suggested by Krezel and Bal [20] for comparison with related values in the literature.

Aqueous Solution Chemistry. Hydrolysis of the Ru^{II} arene halido complexes was monitored by UV-vis spectroscopy. The nature of the hydrolysis products as well as the extent of the reactions were verified by ^1H NMR spectroscopy or HR-MS. For UV-vis spectroscopy the complexes were dissolved in methanol and diluted with H_2O to give 100 μM solutions (5% MeOH/95% H_2O). The absorbance was recorded at several time intervals at the selected wavelength (at which the maximum changes in absorbance were registered) over *ca.* 8–16 h at 310 K. Plots of the change in absorbance with time were computer-fitted to the pseudo first-order rate equation, $A = C_0 + C_1e^{-kt}$ (where C_0 and C_1 are computer-fitted constants and A is the absorbance corresponding to time) using Origin version 8.0 (Microcal Software Ltd.) to give the half-lives ($t_{1/2}$, min) and rate constant values (k, min^{-1}). For ^1H NMR spectroscopy, the complexes were dissolved in MeOD-d_4 and diluted with D_2O to give 100 μM solutions (5% MeOD-d_4/95% D_2O). The spectra were acquired at various time intervals on a Bruker DMX 700 spectrometer (^1H = 700 MHz) using 5 mm diameter tubes. All data processing was carried out using XWIN NMR version 2.0 (Bruker U.K. Ltd.). The relative amounts of Ru^{II} arene halido species or aqua adducts (determined by integration of peaks in ^1H NMR spectra) were quantified.

Rate of Arene Loss. The complexes were dissolved in MeOD-d_4 and diluted with D_2O to give 100 μM solutions (5% MeOD-d_4/95% D_2O). Arene loss over time was followed by ^1H NMR spectroscopy at 310 K for 24 h.

Computational Studies. DFT calculations were carried out using the 2009 version of the Amsterdam Density Functional (ADF) program [21]. Uncontracted Slater Type Orbital (STO) basis sets comprised a triple-ζ plus 5p orbital set (TZP) on Ru with double-ζ plus polarization (DZP) on all other atoms. Default convergence criteria were applied for Self-

Consistent Field (SCF) and cartesian geometry optimizations. For optimizations in internal coordinates, in particular transition state (TS) searches, the angle threshold was set to 1.5° (default = 0.5 º). This criterion was relaxed due to the long bond lengths at the transition states, which make it harder to define torsional terms accurately. The same problem occurs for reactant and product species because the respective entering and leaving groups are included in the calculation, and their relatively weak interaction with the rest of the complex again leads to less well defined torsional terms. However, the energetic consequences of relaxing the angle constraints are negligible. The ADF program reported a single negative eigenvalue in the Hessian matrix for all transition state optimizations. A representative TS was confirmed as a first order saddle point with frequency calculations as described earlier [22]. The conductor-like screening model (COSMO) as implemented in ADF was used to simulate the aqueous environment with ε = 78.4, probe radius = 1.9 Å, and the ND parameter which controls integration accuracy set to 4 (default 3). The atomic radii (Å) used were Ru = 1.950, O = 1.517, C = 1.700, N = 1.608, H = 1.350, Cl = 1.725, Br = 1.850, and I = 1.967.

DFT-Geometry Optimization of DNA Model Nucleobase Adducts. Geometry optimizations were carried out for the 9-EtG and 9-EtA adducts of [(η^6-*p*-cym)Ru(bpm)(9-EtG-*N7*)]$^{2+}$ (**1-9EtG**), [(η^6-*p*-cym)Ru(bpm)(9-EtA-*N7*)]$^{2+}$ (**1-9EtA**), [(η^6-hmb)Ru(bpm)(9-EtG-*N7*)]$^{2+}$ (**8-EtG**), [(η^6-hmb)Ru(bpm)(9-EtA-*N7*)]$^{2+}$ (**8-EtA**) [(η^6-ind)Ru(bpm)(9-EtG-*N7*)]$^{2+}$ (**9-EtG**), [(η^6-ind)Ru(bpm)(9-EtA-*N7*)]$^{2+}$ (**9-EtA**), [(η^6-thn)Ru(bpm)(9-EtG-*N7*)]$^{2+}$ (**10-EtG-*N7***), [(η^6-thn)Ru(bpm)(9-EtG-*N3*)]$^{2+}$ (**10-EtG-*N3***), [(η^6-thn)Ru(bpm)(9-EtA-*N7*)]$^{2+}$ (**10-EtA**), [(η^6-*p*-cym)Ru(phen)(9-EtG-*N7*)]$^{2+}$ (**11-EtG**), [(η^6-*p*-cym)Ru(phen)(9-EtA-*N7*)]$^{2+}$ (**11-EtA**), [(η^6-*p*-cym)Ru(bathophen)(9-EtG-*N7*)]$^{2+}$ (**13-EtG**), and [(η^6-*p*-

cym)Ru(bathophen)(9-EtA-*N7*)]$^{2+}$ (**13-EtA**), for the free 9-ethylguanine and 9-ethyladenine molecules, and for the Ru^{II} arene cations without the bound 9-EtG or 9-EtA. The energies of the separate optimized fragments were subtracted from the energy of the whole Ru^{II} arene nucleobase adducts to obtain the total binding energy of 9-EtG and 9-EtA in each complex.

DNA Binding Kinetics. Calf thymus DNA (CT-DNA) and plasmid DNAs were incubated with the Ru^{II} arene complexes or platinum complexes in 10 mM $NaClO_4$ (pH ≈ 6) at 310 K for 24 h. For each individual assay the values of r_b (r_b values are defined as the number of atoms of the metal bound per nucleotide residue) were determined by Flameless Atomic Absorption Spectrometry (FAAS).

DNA Transcription by RNA Polymerase *In Vitro*. Transcription of the (*Nde*I/*Hpa*I) restriction fragment of pSP73KB DNA with T7 RNA polymerase and electrophoretic analysis of the transcripts were performed according to the protocols recommended by Promega (Promega Protocols and Applications, 43−46 (1989/90)) as previously described [23]. The DNA concentration used was 3.9×10^{-5} M (0.0125 μg /μL) (0.25 μg/sample) (related to the monomeric nucleotide content) and the concentration of complexes was ca. 1.17×10^{-6} M.

Unwinding of Negatively Supercoiled DNA. Unwinding of closed circular supercoiled pUC19 plasmid DNA was assayed by an agarose gel mobility shift assay [24]. The mean unwinding angle can be calculated from the equation $\Phi = -18\sigma/r_b(c)$, where σ is the superhelical density (representing the number of turns added or removed relative to the total number of turns in the relaxed plasmid, indicating the level of supercoiling), and $r_b(c)$

is the r_b value at which the supercoiled and nicked forms comigrate [24]. Samples of plasmid DNA at the concentration of 1.0×10^{-4} M (0.032 μg/μL) (0.5 μg/ sample) (related to the monomeric nucleotide content) were incubated with the Ru^{II} arene complexes at 310 K for 24 h. All samples were precipitated by ethanol and redissolved in the TAE (Tris-aceate/EDTA, pH = 8.0) buffer to remove free, unbound Ru^{II} arene complexes. One aliquot of the precipitated sample was subjected to electrophoresis on 1% agarose gels running at 298 K with TAE buffer and the voltage was set at 25 V. The gels were then stained with ethidium bromide (EtBr), followed by photography with a transilluminator. Electron Absorption Spectrometry (EAS) and FAAS were used for the determination of r_b values.

Circular Dichroism (CD). Isothermal CD spectra of CT-DNA modified by the Ru^{II} arene complexes at a concentration of 3.3×10^{-4} M were recorded at 298 K in 10 mM $NaClO_4$ by using a Jasco J-720 spectropolarimeter equipped with a thermoelectrically controlled cell holder. The cell pathlength was 1 cm. CD spectra were recorded in the range of 230−600 nm in 0.5 nm increments with an averaging time of 0.5 s.

Flow Linear Dichroism (LD). Flow LD spectra were collected by using a flow Couette cell in a Jasco J-720 spectropolarimeter adapted for LD measurements. The flow cell consists of a fixed outer cylinder and a rotating solid quartz inner cylinder, separated by a gap of 0.5 mm, giving a total pathlength of 1 mm. LD spectra of DNA at the concentration 3.3×10^{-4} M modified by the Ru^{II} arene complexes were recorded at 298 K in 10 mM $NaClO_4$.

Other Physical Methods. The FAAS measurements were carried out on a Varian AA240Z Zeeman atomic absorption spectrometer equipped with a GTA 120 graphite tube atomizer.

The PAA gels were visualized by using a BAS 2500 FUJIFILM bioimaging analyzer, with the AIDA image analyzer software (Raytest, Germany).

Cancer Cell Growth Inhibition. After plating, human ovarian A2780 and cisplatin-resistant A2780cis cancer cells were treated with Ru^{II} arene complexes on day 3, and human lung A549 and human colon HCT116 cancer cells on day 2, at concentrations ranging from 0.1 to 100 μM. Solutions of the Ru^{II} complexes were made up in 0.125% DMSO to assist dissolution (0.03% final concentration of DMSO per well in the 96-well plate). Cells were exposed to the complexes for 24 h, washed, supplied with fresh medium, allowed to grow for three doubling times (72 h), and then the protein content measured (proportional to cell survival) using the sulforhodamine B (SRB) assay [25].

Reactions with Glutathione (GSH). A solution containing [(η^6-*p*-cym)Ru(bpm)Cl][PF_6] (**1**) (100 μM) and GSH (10 mM) was incubated at 310 K in D_2O and the changes monitored by ^{1}H NMR and UV-vis spectroscopy for 24 h.

Results and Discussion

Synthesis and Characterization. The [(η^6-arene)Ru(*N,N'*)X]$^{n+}$ complexes studied in this work are shown in Figure 1. The monocationic Ru^{II} arene halido complexes **1**−**13** and the 9-EtG-*N7* complex **14** were synthesized as PF_6 salts in good yields (>50% in almost all cases). All the complexes were fully characterized by 1D and 2D ^{1}H NMR methods as well as 1D ^{13}C NMR. The molecular structures of complexes **3**, **4**, **6**, **7** and **14** were determined by single crystal X-ray diffraction. The molecular structure of complex **1** has previously been published [14b]. Selected bond lengths and angles are given in Table 1, the structures with numbering schemes are shown in Figure 2 and the crystallographic data are listed in Table S1. In all cases, the complexes adopt the familiar pseudo-octahedral three-legged

piano stool geometry common to all other Ru^{II} arene structures [26] with the Ru^{II} atom π-bonded to the corresponding arene ligand (*p*-cym in **3** and **14**; bip in **4** and **6**; or etb in **7**), coordinated to a chloride (**4** and **7**), to an iodide (**3** and **6**), or to *N7* of 9-EtG (**14**), and to two nitrogen atoms of the chelating ligand 2,2'-bipyrimidine (bpm) which constitute the three legs of the piano stool.

The values for Ru–$arene_{(centroid)}$ bond lengths are comparable to analogous Ru^{II} arene complexes containing *N,N′* chelated ligands [27, 56]. Neither the nature of the corresponding *N,N′* chelating ligand, the arene nor the halogen greatly influences the corresponding Ru–$arene_{(centroid)}$ distances (ca. 1.70 Å).The corresponding Ru–I bond lengths in **3** and **6** are also within the same range (ca. 2.7 Å) and are slightly shorter compared to other Ru^{II} arene complexes containing iodide as a leaving group [28, 29, 30]. Similarly, the Ru−Cl bond lengths are almost the same (ca. 2.4 Å). The Ru(1)−$N(1)_{(bpm)}$ and Ru(1)−$N(8)_{(bpm)}$ bond lengths in these arene complexes are ca. 2.09 Å. For the four halido complexes, the Ru–*N,N′* bond lengths are significantly longer than those found in the crystal structures of similar arene Ru^{II} arene bipyridine complexes [31]. The N(1)−Ru(1)−N(8) bond angles in complexes **3**, **4**, **6**, **7**, and **14** do not differ significantly from each other. In the case of complex [(η^6-bip)Ru(bpm)Cl][PF_6] (**4**) , the Ru^{II} molecules lay back-to-back with an adjacent complex in an intermolecular π-π stacking interaction. (Figure S1). The X-ray crystal structures of compounds **3**, **4**, **6** and **7** show an increased number of intra and/or intermolecular π-π stacking interactions, particularly for complexes **4** and **6** (Figure S2), which contain bip as the arene. Their crystal packing also displays strong H-bonding throughout the unit cell, which is a common feature observed in similar Ru^{II} arene complexes containing extended aromatic rings [32]. For complex **7**, CH-π

interactions between the C−H protons of one of the pyrazine rings in the 2,2'-bipyrimidine (bpm) chelating ligand and the centroid of one of the pyrazine rings in the bpm belonging to a neighboring molecule were observed. (Figure S3). The occurrence of CH-π interactions is now well established [33] and the interaction ranges from weak (CH···π centre 2.6–3.0 Å) to very strong (CH···π centre < 2.6 Å) [34]. Such interactions can play an important role in protein stability and in recognition processes. The CH···π interactions observed for complex **7** (2.9 Å) are within the weak-interaction range. The Ru–$N7_{(9\text{-EtG})}$ bond distance in the guanine adduct **14** (2.1125(19)Å) is similar to those in related organometallic Ru^{II} guanine adducts [26]. There are multiple H-bonding interactions throughout the crystal. The main fragments involved are bpm, 9-EtG, and solvent molecules (water), Figure S4. Such aggregations have been observed in a number of Ru^{II} and Pt^{II} crystal structures containing purine derivatives [35]. Water can play an important role in intercalation modes; specific binding of water to DNA complexes can make a significant contribution to the free energy of drug binding [36]. The 9-EtG adduct (**14**) was also characterized by ^{1}H NMR spectroscopy; Figure S5 shows its 2D ^{1}H-^{1}H NOESY spectrum. An NOE cross-peak between H8 of bound 9-EtG and the 2,2'-CH in bpm was observed, suggesting that these two atoms are in close proximity (as previously observed in analogous Ru^{II} arene complexes) [5, 37].

Aqueous Solution Chemistry. Dissolution of compounds **1**–**13** in 5% MeOH/95% H_2O at 310 K gave rise to ligand exchange reactions as indicated by the concomitant changes in UV-Vis absorption bands. The time-evolution spectra for all the Ru^{II} arene complexes at 310 K are shown in Figure S6. The time dependence of the absorbance of all the complexes at selected wavelengths followed pseudo first-order kinetics in each case. The

corresponding rate constants and half-lives are listed in Table 2. The dependence of the absorbance at 332 nm over *ca.* 16 h during aquation of [(η^6-*p*-cym)Ru(bpm)Cl][PF_6] (**1**) at 310 K is shown in Figure S7.

In order to characterize the products of hydrolysis and to determine the extent of the reactions, freshly-made 100 μM (5% MeOD-d_4/95% D_2O) solutions of complexes **1**−**13** were allowed to equilibrate for 24−48 h at 310 K and were then studied at the same temperature using ^{1}H NMR spectroscopy. The ^{1}H NMR spectra of complexes **1**−**11** and **13** initially contained one major set of peaks (halido species) and then a second set of peaks increased in intensity with time. The new set of peaks had the same chemical shifts as those of the aqua adducts (prepared independently) under the same conditions (ca. 100 μM solutions (5% MeOD-d_4/95% D_2O) at 310 K). The mass-to-charge ratios and isotopic models obtained from HR-MS spectra were consistent with the formation of the aqua adducts, Table S2. Table 3 summarizes the equilibrium constants (calculated by integration of ^{1}H NMR signals) after 24 h of reaction for complexes **1**−**11** and **13**. For complexes [(η^6-bip)Ru(bpm)Cl][PF_6] (**4**), [(η^6-bip)Ru(bpm)Br][PF_6] (**5**), [(η^6-etb)Ru(bpm)Cl][PF_6] (**7**), and [(η^6-*p*-cym)Ru(phendio)Cl][PF_6] (**12**) an additional set of peaks was also observed corresponding to the products which had undergone arene loss during the aquation. In the case of complex **12**, it was observed that it displayed a complicated ^{1}H NMR spectrum upon dissolution which could not be explained by hydrolysis alone.

Within the series of complexes having *p*-cym as arene and bpm as chelating ligand, the hydrolysis reactions of the chlorido (**1**) and bromido (**2**) complexes are more thermodynamically favored (K = 790.6 and 280.5 μM, respectively) compared to that of the iodido complex (**3**) (K = 14.0 μM). Similarly, in the bip/bpm series it was found that the

chlorido (**4**) and bromido (**5**) complexes hydrolyzed to a larger extent (K = 9.0 and 10.4 μM, respectively) than the analogous iodido (**6**) complex (K = 0.2 μM). For complexes **1**, **11**, and **12**−**13** where *p*-cym (arene) and Cl (leaving group) are kept constant but the chelating ligand is varied, the amount of aqua adduct (and equilibrium constant) determined by ^{1}H NMR increases in the order bathophen (**13**) < phen (**11**) < bpm (**1**). When the chelating ligand is bpm and the leaving group as Cl, the extent of hydrolysis decreases with arene in the order *p*-cym (**1**) > thn (**10**) > ind (**9**) > hmb (**8**) > etb (**7**) > bip (**4**).

Complexes **2**, **5**, **7**−**9** and **11**−**13** undergo relatively fast hydrolysis with half-lives of < 60 min at 310 K. The reported half-lives of aquation of the previously reported chlorido ethylenediamine (en) Ru^{II} arene complexes, [(η^6-dha)Ru(en)Cl][PF_6], [(η^6-tha)Ru(en)Cl][PF_6] and [(η^6-bip)Ru(en)Cl][PF_6] [38] are 10–80 times smaller than those of these complexes under comparable conditions. Within the *p*-cym/Cl series containing various chelating ligands, the presence of a better π-acceptor chelating ligand reduces the electron-density on the Ru^{II} centre, making it less favorable for the chlorido ligand to leave, thus slowing down the hydrolysis reaction. Thus the rates increase in the order **1** (bpm) < **12** (phendio) < **11** (phen) < **13** (bathophen). The fact that the substituent heteroatoms on the chelating ligands (such as the extra pair of nitrogens in 2,2'-bipyrimidine (bpm) or two oxygens in 1,10-phenanthroline-5,6-dione (phendio)) which are electron donors [39] may contribute to stabilization of the Ru−Cl bonds by π-back donation. Previous work [40] has shown that an *N,N′* chelating group such as 2,2'-bipyridine (bpy) slows down substitution of the aqua ligand in [(η^6-C_6H_6)Ru(bpy)(OH_2)]$^{2+}$ just as the replacement of ethylenediamine (en) by acetylacetonate (acac) to form [(η^6-arene)Ru(acac)]$^{+}$ complexes accelerates hydrolysis. Within the Ru^{II} arene bpm/Cl series, it was observed that the incorporation of

arenes with either an increased aromatic character or electron-withdrawing substituents in the coordinated ring, significantly decreases the rate of the hydrolysis reaction in the order **7** (etb) > **8** (hmb) > **9** (ind) > **10** (thn) > **1** (*p*-cym) > **4** (bip). Bip has a high aromaticity and competes as a π-acceptor [41] with the chelating ligand (bpm) for electron density. This leads to a weakening of the corresponding Ru−arene bonds and consequently to the complete loss of the bip in the case of complex **4**. No arene loss is observed in the case of the complexes bearing other arenes, all of which have electron donating aliphatic substituents on the ring. A similar arene loss was previously observed for other Ru^{II} bip complexes containing phenylazopyridines as π-acceptor ligands [42]. Within this same series of complexes **1**−**6**, it can also be noticed that a combination of a large leaving group (such as I) and a large arene (such as bip) in complexes **3** and **6** together make the Ru^{II} centre less accessible to an incoming ligand. This effect corresponds to the experimental observation of a very slow hydrolysis rate. The inclusion of a more electronegative halide (like Cl or Br in **1** and **2** or **4** and **5**) leads to an increase in the hydrolysis rate when compared to the iodido derivatives, which is enhanced when the arene is replaced by a less sterically-demanding ligand such as *p*-cym in complexes **1**−**3**. Arene ligands such as benzene (bz) are reported to exhibit a strong *trans*-labilizing effect for the aqua ligand in $[(\eta^6\text{-bz})Ru(OH_2)_3]^{2+}$ [43]. This class of strong π-acid ligands is able to accept electron density from the central Ru^{II} atom giving rise to a higher charge on the metal. Acidic hydrolysis of Ru^{III} complexes such as $[Ru(NH_3)_4(X)_2]^+$ and $[Ru(NH_3)_5X]^{2+}$ (X is Cl, Br, and I) occurs *via* an associative pathway in which bond-making is more important than bond-breaking [44].

Additionally, the changes in the ^{1}H NMR chemical shifts of the aromatic protons in either the corresponding arene rings or the corresponding *N,N′* chelating ligands of the aqua

adducts of complexes **1, 8-11** and **13** present in an equilibrated 100 μM (D_2O) solution at 310 K were followed with change in pH* over the range *ca.* 1 to 12. Figure S8 shows how the peaks shift to higher field due to deprotonation of the bound water molecule in the aqua adduct of complex **1**, $[(\eta^6\text{-}p\text{-cym})Ru(bpm)(OH_2)]^{2+}$, but do not change in intensity as an indication that no other species are being formed. The pK_a* values for complexes **1**, **8**,**9**, and **11** are listed in Table 4. For complexes **1** (*p*-cym/bpm), **8** (hmb/bpm), **9** (ind/bpm), and **11** (*p*-cym/phen) the pK_a* values are in the range from 6.91 to 7.32 and are all significantly lower (*ca.* 1.5 units) than those reported for analogous $[(\eta^6\text{-arene})Ru(N,N')(OH_2)]^{2+}$ complexes [6b, 45]. Such a decrease in acidity has been attributed before to an increased electron density on the metal centre favored by a combination of electron-donating/π-acceptor−arene/chelating ligands. Complexes **1**, **8**, **9**, and **11** will therefore be present as a mixture of aqua and (less reactive) hydroxido adducts at pH 7.4.

Mechanism of Hydrolysis. Density Functional Theory (DFT) computational methods were employed to obtain information about the influence of the leaving group on the mechanism of hydrolysis for the *p*-cym/bpm series of Ru^{II} arene complexes **1**−**6**. A test of the structural accuracy of the functional PW91 with COSMO solvation was performed by comparing the fully optimized structures of the cations in complexes **1**–**6** with the corresponding X-ray crystal structures of **1** [14b], **3**, **4** and **6**. The functional PW91 was found to overestimate the Ru^{II} bond lengths by *ca.* 0.01−0.04 Å, particularly for the computed Ru−X distances (~2.44 Å), which were ca. 0.05 Å longer than those found in the solid state. However, the overall agreement with the experimental data was satisfactory. A scheme for the reaction modeled is shown in Figure 3. For each of the resting states ([RS] = $\{[(\eta^6\text{-arene})Ru(bpm)X]^{+}\cdot H_2O]\}$) and the corresponding products ([P] = $\{[(\eta^6\text{-}$

arene)Ru(bpm)$(OH_2)]^{2+}\cdot X^-]\}$), the entering (H_2O) and the leaving groups (X^-) are retained within the second coordination sphere of the Ru^{II} centre. Complex **1** was chosen as a model system; based on previously reported work [6b] on analogous Ru^{II} arene complexes. A full geometry optimization of its transition state ([TS]) was performed starting from Ru–Cl and Ru–OH_2 distances of 3.200 Å and 2.899 Å, respectively, in the initial geometry. The optimised structure for the [TS] for the Ru^{II} arene cation $[(\eta^6$-*p*-cym)Ru(bpm)Cl$]^+$ is shown in Figure 4. The geometry-optimized structure in the [TS] of the Ru^{II} arene cation in complex **1**, gave Ru–Cl and Ru–OH_2 distances of 3.11 Å and 2.68 Å, respectively. The corresponding energy value determined for the [TS] (–6657.51 kcal mol^{-1}) was found to be 20.1 kcal mol^{-1} larger than that for the chlorido compound in the [RS]. Given that the hydrolysis reaction could be assumed to be either an associative, a dissociative, or an interchange (I_a or I_d) process, a frequency calculation was performed for the [TS] of the Ru^{II} arene cation in complex **1**. Two imaginary frequencies were retrieved from the computation, –152 and –20 cm^{-1}. The latter is small and arises from the numerical noise inherent in the finite difference method required when a COSMO field is enabled. The former (and more significant) frequency value (–152 cm^{-1}) gave a vibrational mode where the entering water molecule (H_2O) and leaving halido ligand (Cl^-) are moving in a concerted process consistent with an associatively activated reaction. The corresponding scaled displacement vectors are shown in Figure S9. Under the assumption that the same associative hydrolysis mechanism applies for other related systems, the effect of varying X and the arene was explored. The results are listed in Table 5, from where it can be seen that the corresponding barrier heights do not vary significantly when the arene *p*-cym (in complexes **1**, **2**, and **3**) is substituted by bip (in complexes **4**, **5**, and **6**). The forward

reaction barriers and overall reaction energies for the aquation of the corresponding halido ligand (Cl, Br, or I) follow the increasing order Cl ≈ Br < I, and *p*-cym < bip.

The transition state obtained from density functional theory (DFT) calculations, suggested that aquation of the $[(\eta^6\text{-arene})Ru(bpm)X]^+$ complexes where arene is *p*-cym (**1**−**3**) or bip (**4**−**6**) and X is Cl, Br, or I, proceeds *via* a concerted interchange (associative) mechanism rather than a stepwise dissociation/coordination process (dissociative). For the *p*-cym/bpm series of complexes (**1**−**3**) the reaction does not appear to be strongly associatively nor dissociatively activated, because the corresponding Ru–X bonds at the transition state extend by ~0.66, 0.71, and 0.81 Å for Cl, Br, and I, respectively, relative to the reactant species. In the case of the corresponding Ru–O bonds in the transition state, it was found that they are ca. 0.50 Å longer than in the aqua products in the three cases. The results for the bip/bpm series of complexes (**4**−**6**) showed that the hydrolysis might not be strongly associatively nor dissociatively activated either. The corresponding Ru–X bonds at the transition state extend by ca. 0.58, 0.61, and 0.69 Å for Cl, Br, and I, respectively, relative to the reactant species, whereas the Ru–O bonds in the transition state were found to be ca. 0.55 Å longer than in the aqua products. Given that Ru–X bond-breaking alone is not the rate-controlling step in the associative pathway, a heavier (and larger) halide will impede the access of the H_2O molecule to the central Ru^{II} atom in associative states. This hypothesis is in good agreement with the experimental observation that complexes **3** and **6** (bearing I as the leaving group) display the slowest rates of hydrolysis within the corresponding series. This assumption has also been suggested for Ru complexes displaying higher coordination numbers (i.e. seven) [46]. The calculated reaction barriers and overall reaction energies for the aquation of the halido complexes **1**–**6** follow the

increasing order Cl ≈ Br < I. However, the effect of different halides on the experimental hydrolysis rates of these Ru^{II} arene complexes differs from the calculation and follows the increasing order Br < Cl < I. This trend has been experimentally observed before for platinum compounds of the type $[PtX_n(OH_2)_{4-n}]^{(2-n)+}$, for which Br analogues of Cl complexes hydrolyze faster in all three hydrolysis steps [27]. The calculated higher activation energies might be responsible for the observed slower hydrolysis of the iodido complexes during the associative ligand interchange in each series. Furthermore, the electron-accepting effect of strong π-acid arene ligands might be responsible for the shift toward a more associative pathway in the $I_d \leftrightarrow I_a$ mechanistic continuum for the $[(\eta^6\text{-}p\text{-cym})Ru(N,N')Cl]^+$ complexes studied herein. The accuracy of the calculation was not sufficient to account for the differences found experimentally in the hydrolysis rates between the chlorido and bromido complexes.

Interactions with Nucleobases. Interactions of several complexes with 9-EtG and 9-EtA were studied by multidimensional ^{1}H NMR spectroscopy and the nature of the products was verified by HR-MS. All the reactions were carried out in NMR tubes in D_2O and followed over 48 h at 310 K. Figure 5 shows the reaction of complex **11** with 9-EtG as an example. The ^{1}H NMR peaks corresponding to H8 in all the 9-EtG-*N7* adducts are shifted to high field (ca. 0.5 ppm) relative to free 9-EtG under the same conditions. Often, metallation at the *N7* site of purine bases produces a low field shift of the H8 resonance by about 0.3–1 ppm [47, 48]. This effect has also been observed before for analogous Ru^{II} arene complexes containing bpy[Error! Bookmark not defined.] or acac [6a] as the chelating ligands. The compounds studied in this work showed significant and rapid binding to 9-EtG-*N7* (detectable after *ca*. 10 min and to *ca*. 34–94% extent). The reactions of complexes $[(\eta^6\text{-}p\text{-}$

cym)Ru(bpm)Cl)]$^{+}$ (**1**), [(η^6-thn)Ru(bpm)Cl)]$^{+}$ (**10**) and [(η^6-*p*-cym)Ru(bathophen)Cl)]$^{+}$ (**13**) required *ca.* 8 h to reach equilibrium in each case. However, a different behavior was observed for complexes [(η^6-hmb)Ru(bpm)Cl)]$^{+}$ (**8**) and [(η^6-ind)Ru(bpm)Cl)]$^{+}$ (**9**), which reacted with 9-EtG much faster, reaching equilibrium after 56 and 52 min, respectively. Table S6 lists the percentage of species present in solution for the reactions of complexes **1**, **8**–**11**, and **13** with 9-EtG after selected times. The reactions of complexes **8**, **9**, and **10** with 9-EtG were found to produce higher yields. Interestingly, for complex [(η^6-thn)Ru(bpm)Cl][PF_6] (**10**) ca. 12% of a second guanine-bound species (possibly [(η^6-thn)Ru(bpm)(9-EtG-*N3*)]$^{2+}$) was also detected at equilibrium (*ca*. 510 min), Figure S10. The mass-to-charge ratios and isotopic models obtained from HR-MS spectra were consistent with the formation of the guanine adducts as the corresponding products of the individual reactions, Table S3. The addition of an equimolar amount of 9-EtA (100 μM) to freshly-prepared D_2O solutions of the complexes at 310 K resulted in no new species even after 48 h.

Since nucleobase binding is likely to require initial hydrolysis, the slow aquation rates and reduced extent of hydrolysis of these complexes at equilibrium may account for the observed extent of nucleobase binding. The calculated binding energies for 9-EtG in the corresponding nucleobase adducts appear to be related to the trend determined for the extent of nucleobase binding (*vide infra*). None of the Ru^{II} arene complexes **1**, **8**–**11**, and **13** showed evidence of binding to 9-ethyladenine. These complexes display a more discriminating behavior towards binding to purine bases when compared to cisplatin, for which binding to adenine is also observed [49]. It has been found that H-bonding from C6O in guanine to N–H protons in the bidentate chelating ligand ethylenediamine (en),

contributes to the high preference for binding of $\{(\eta^6\text{-arene})Ru(en)\}^{2+}$ to guanine versus adenine. However, replacement of en (NH as H-bond donor) by bpm (no NH) in these series of complexes did not change the selectivity for guanine bases.

In order to gain further insight into the nature and relative stabilities of the guanine and adenine adducts of the Ru^{II} arene complexes **1**, **8**−**11**, and **13**, their optimized geometries were obtained using DFT calculations. Their minimum energy structures are shown in Figures S11 and S12 (for the 9-EtG-*N7* and the 9-EtA-*N7* adducts, respectively). The total binding energies for both nucleobases are shown in Table 6. The binding energies include a COSMO contribution which simulates an aqueous environment. Under these conditions, the binding of 9-ethylguanine was found to be more favorable than that of 9-ethyladenine by ca. 10.0 kcal mol^{-1}. Furthermore, the nucleobase 9-ethylguanine shows significant binding energies towards all compounds (≥38.5 kcal mol^{-1}), the largest value being for the adduct $[(\eta^6\text{-thn})Ru(bpm)(9\text{-EtG-}N7]^{2+}$ (**10-9EtG**) with a value of 41.0 kcal mol^{-1}. In the case of 9-ethyladenine, a smaller binding energy towards all compounds (≤34.4 kcal mol^{-1}) was found; the largest energy was calculated for the adduct $[(\eta^6\text{-thn})Ru(bpm)(9\text{-EtA-}N7]^{2+}$ (**10-9EtA**). The binding of 9-EtG to the *N3* position in complex **10** was also investigated. The minimum energy structures are shown in Figure S13 for both the 9-EtG-*N7* and 9-EtG-*N3* adducts. The calculated total binding energies are 41.0 and 18.5 kcal mol^{-1} for the 9-EtG-*N7* and the 9-EtG-*N3* adduct, respectively.

Despite the lack of cytotoxic activity, compounds **1**, **8**, **9**, and **10** showed a significant calculated binding energy for 9-EtG-N7 (ca. 38.8 kcal mol–1). As would be expected, the binding of 9-EtG to complex **10** through *N7* is ca. 20 kcal mol^{-1} more stable than the binding through *N3*. The calculations were also able to reproduce the H-bond

distance ($CH_{(N,N'\text{-chelating})}\cdots O_{(9\text{-EtG})}$) found in the X-ray crystal structure of the 9-EtG adduct, complex **14** within sufficient accuracy. Therefore, it is assumed that the analogous values from the DFT-optimised geometries for the rest of the 9-EtG adducts of complexes **1**, **8**–**11** and **13** will also be within the expected ranges. The calculations predict $CH_{(N,N'\text{-chelating})}\cdots O_{(9\text{-EtG})}$ distances within the range of 2.20–3.11 Å and $C–H_{(N,N'\text{-chelating})}\cdots O_{(9\text{-EtG})}$ angles within 114.93–134.97º. The shortest H-bond distance was found for the 9-EtG adduct of complex **10**, which might explain the high binding energy calculated for this adduct.

DNA Binding Reactions in Cell-Free Media. In order to explore the possibility of DNA as a potential target, two complexes [(η^6-*p*-cym)Ru(bpm)Cl][PF_6] **(1)** and [(η^6-*p*-cym)Ru(phen)Cl][PF_6] (**11**) were selected for further studies of CT-DNA interactions in cell-free media. The results of the DNA binding experiments are summarized in Table 7. Both complexes reacted with CT-DNA to a moderate extent and the reactions were complete after *ca*. 20 h. Complex **11** was found to bind much faster and to a larger extent than complex **1**, with equilibrium for complex **11** being reached within the first 1.5 h. After 24 h of reaction both complexes has reacted to a similar, ca. 60%, Figure S14. The dialysis experiments against two different sodium salts indicate that the coordination of the Ru^{II} arene complexes to CT-DNA is reversible and dependent on the nature of the salt. In the case of [(η^6-*p*-cym)Ru(phen)(Cl)][PF_6] (**11**), dialysis either against 10 mM $NaClO_4$ or 0.1 M of NaCl resulted in a decrease in the percentage of complex bound to DNA by ca. 20%. For complex **1**, dialysis against 10 mM $NaClO_4$ did not change the percentage of complex bound to DNA whereas dialysis against 0.1 M of NaCl reduced the amount to the same extent as for complex **11** (ca. 20%).

Further investigations were aimed at identifying the Ru binding sites in natural DNA for the reactions of [(η^6-*p*-cym)Ru(bpm)Cl][PF_6] (**1**) and [(η^6-*p*-cym)Ru(phen)Cl][PF_6] (**11**). The autoradiogram of the inhibition of RNA synthesis by T7 RNA polymerase on pSP73KB DNA containing adducts of the Ru^{II} arene complexes or cisplatin is shown in Figure 7. The bands corresponding to the transcription of DNA modified by complexes **1** and **11** yielded fragments of newly synthesized RNA of defined sizes, which indicates that RNA synthesis on these templates was prematurely terminated. The major stop sites occurred at similar positions in the gel and were solely at guanine residues, for both Ru^{II} arene complexes, Figure 8.

Intensities of the bands corresponding to the transcription of DNA modified by complex **11** are considerably weaker than those of the bands corresponding to the transcription of DNA modified by complex **1** (Figure 7). This may indicate that efficiency of DNA adducts of **11** to prematurely terminate RNA synthesis by T7 RNA polymerase is lower than that of DNA adducts of **1**. We can speculate that this reduced efficiency is associated with lesser distortion of DNA conformation exerted by DNA adducts of **11** (compared to DNA adducts of **1**) as deduced from the results of CD spectroscopy of DNA modified by these complexes (Figure 10). Another possibility might be through the labilization of DNA-metal adducts by 1,10-phenanthroline chelating ligand in **11** being greater than that exerted by 2,2'-bipyrimidine chelating ligand in **1** due to the introduction of electron withdrawing substituents in the 4,4' positions of bpm in complex **11** (which contains 1,10-phenanthroline chelating ligand). As a consequence, some molecules of **11** originally bound to DNA might be displaced by T7 RNA polymerase during transcription of the template strand containing them and consequently would be unable to prematurely terminate RNA synthesis by this

enzyme. The labilization of other metal-biologically relevant molecules by spectator ligands (in metal complexes) has already been demonstrated for Pt(II) complexes[50].

The rate of binding to DNA for complex **1** is slower than that determined for the anticancer drug cisplatin ($t_{1/2}$ *ca.* 2 h under similar conditions) [51], for which DNA binding is thought to be responsible for its cytotoxic properties. Interestingly, the corresponding binding rate for complex **11** was found to be in the same range as that of cisplatin. In contrast, other Ru^{II} arene analogues i.e. $[(\eta^6\text{-bip})Ru(en)Cl]^+$, which has also been shown to be cytotoxic to cancer cells [26a, 52], react much more rapidly with DNA under similar conditions ($t_{1/2}$ *ca.* 10 min).

The native agarose gels resulting from DNA modified by complexes $[(\eta^6\text{-}p\text{-cym})Ru(bpm)Cl][PF_6]$ (**1**) and $[(\eta^6\text{-}p\text{-cym})Ru(phen)Cl][PF_6]$ (**11**) are shown in Figure 9. The DNA unwinding angles produced by the adducts of **1** and **11** were determined to be 7.7° and 6.6°, respectively, which is consistent with only a small reduction of the intensity of the negative CD band at ca. 245 nm of DNA modified by **1** or **11** (*vide infra*) [53]. This is smaller than that observed for the Ru^{II} arene complexes $[(\eta^6\text{-arene})Ru(en)Cl]^+$ (range 7–14°) [30] and resembles more those produced by monofunctional cisplatin adducts (6° and 13° for mono or bifunctional adducts, respectively) [54]. The co-migration point of the modified supercoiled and nicked DNA (r_b(c)) was reached at r_b = 0.13 and 0.15 (for **1** and **11**, respectively) as shown in Table 8

The DNA binding after hydrolysis of the Ru^{II} arene complexes **1** and **11** results in a mild degree of unwinding (7–8°). This relatively small DNA unwinding is very similar for the two complexes, but even smaller than that observed for $[(\eta^6\text{-arene})Ru(en)Cl]^+$ complexes (range 7–14°) [30].

CD spectra of CT-DNA modified by complexes (**1**) and (**11**) (at 298 K in 10 mM $NaClO_4$) were also recorded at r_b values in the range of 0.013−0.047. As can be seen from Figure 10, small changes in the CD spectrum at wavelengths below 300 nm are observed upon interaction of complex **1** (and to a much lesser extent of complex **11**) with CT-DNA. As a consequence of the ruthenation of CT-DNA, the intensity of the positive CD band at around 280 nm increases for complex **1** whereas the CD spectrum recorded for CT-DNA modified by **11** remains unchanged. The signature of complexes **1** and **11** bound to CT-DNA includes no ICD. The changes in CD spectra of CT-DNA (monitored at 246 and 278 nm) modified by Ru^{II} arene complexes **1** and **11** (at different r_b values) are shown in Table S4.

CD spectra showed that the binding of **1** (and to a lesser extent of **11**) to DNA results in subtle conformational alterations in DNA that could be related to a denaturational character, similar to those induced in DNA by clinically ineffective transplatin. It is possible that these changes could also be associated with the bound Ru arene fragment given that these Ru^{II} arene complexes show maxima in the proximity of a DNA maximum.

Overall, these combined results might suggest the presence of combined covalent (coordinative), non-covalent intercalative, and monofunctional coordination binding modes of DNA binding for complexes **1** and **11** upon hydrolysis.

Binding of the Ru^{II} arene complexes to CT-DNA was also monitored by linear dichroism spectroscopy (LD). It is well established that the magnitude of the LD signal measured within the DNA absorption band (i.e. at the 258 nm maximum) is a function of its persistence length [55]. The magnitudes of the LD signals at 258 nm decrease as a function of r_b for the Ru^{II} arene complexes **1** and **11**, Figure 11. The changes in LD spectra of CT-DNA modified by the Ru^{II} complexes at different r_b values were monitored at 258.5 nm,

Table S5. It can be seen that both complexes behave similarly and their changes are within the same range. These results might suggest that the formation of DNA adducts could be eventually accompanied by the appearance of flexible hinge joints at the site of the lesion.

Cancer Cell Growth Inhibition The halido complexes **1**−**6** (Figure 1) were tested against the A2780 human ovarian, A2780 cisplatin resistant human ovarian, A459 human lung, and HCT116 human colon cancer cell lines, whereas the remaining halido complexes **8**−**11** and **13** were tested against the A2780 human ovarian cancer cell line. Strikingly, all the bpm-containing complexes **1**−**6** and **8**−**10** displayed IC_{50} values larger than 100 μM against the corresponding cell lines tested (IC_{50} value for cisplatin was 1.0 μM under the same conditions). Complexes **11** and **13**, bearing phen and bathophen as the chelating ligand, respectively, were cytotoxic to A2780 human ovarian cancer cells, Table 9. The most active complex is [(η^6-*p*-cym)Ru(bathophen)Cl][PF_6] (**13**) with an IC_{50} value of 0.5 μM, comparable to that of cisplatin (IC_{50} for cisplatin 1.1 μM under the same conditions). The IC_{50} for [(η^6-*p*-cym)Ru(phen)Cl][PF_6] (**11**) against this cancer cell line was 23 μM.

A loss of cytotoxicity towards cancer cells has been previously observed for complexes of the type [(η^6-arene)Ru(en)Cl]$^+$ when en, a σ-donor, is replaced by 2,2'-bipyridine [56], a strong π-acceptor. Changing the electronic features of the chelating ligands by incorporating electron donating heteroatoms in the 4,4' positions of bpm (such as in the phendio complex **12**) did not restore the cytotoxic activity. From a structural point of view, loss of activity in these derivatives could arise from the absence of $N_{(sp^3)}H$ groups, which are known to stabilize nucleobase adducts through strong H-bonding between an NH of en and C6O from the guanine (G) nucleobase [57]. The electronic properties of the complexes might also account for the observed loss of activity; metal-DNA bonds have been shown to

be labilized by heteroarene ligands..After substitution of two water molecules by thiourea (tu) for instance, labilization of the Pt–N bond in the trans position forms a ring-opened trisubstituted $[Pt(tu)_3(N\text{-}N_{open})]^{2+}$ species [**Error! Bookmark not defined.**]. Similar reactions are also known in the biotransformation pathway of cisplatin;where the resulting products are inert to further substitution reactions and therefore limit the active concentration of the drug.[58]

Interactions with GSH. ^{1}H NMR and UV-vis absorption spectra of solutions containing the inactive complex $[(\eta^6\text{-}p\text{-cym})Ru(bpm)Cl][PF_6]$ (**1**) (100 μM) and a 100-fold molar excess of GSH (10 mM, to mimic intracellular conditions) were acquired over 24 h at 310 K. The time evolution spectra for the Ru^{II} arene complex **1** are shown in Figure S15. The ^{1}H NMR spectra of complex **1** initially contained one major set of peaks (chlorido species) and then a second set of peaks assignable to the aqua adduct $[(\eta^6\text{-}p\text{-cym})Ru(bpm)OH_2]^{2+}$, increased in intensity with time. A third set of peaks attributable to the G*S*-bound ruthenium adduct was also detected $[(\eta^6\text{-}p\text{-cym})Ru(bpm)GS]^+$ (**1-G*S***), Figure 12. The mass-to-charge ratio and isotopic model obtained from HR-MS spectra were consistent with the formation of the tripeptide-substituted Ru^{II} product; and the calculated *m/z* value for $C_{28}H_{36}N_7O_6RuS$ (700.1508), found *m/z* (700.1493). Some sulfur-bound thiolate adducts with platinum anticancer drugs are formed irreversibly and are also largely unreactive (e.g. towards DNA binding) [59].

Conclusions

We have shown here that several 2,2'-bipyrimidine (bpm) complexes $[(\eta^6\text{-arene})Ru(bpm)Cl][PF_6]$ are inactive as anticancer agents towards human ovarian cancer

cells. However a change in the chelating ligand from bpm to 1,10-phenanthroline (phen) or 4,7-diphenyl-1,10-phenanthroline (bathophen) leads to activity. Significant changes in the chemical reactivity of the compounds towards hydrolysis are also observed; the hydrolysis rates of $[(\eta^6\text{-arene})Ru(N,N')X]^+$ complexes vary over a wide range, from half-lives of minutes (14.5 min for complex $[(\eta^6\text{-etb})Ru(bpm)Cl]^+$ (**7**)) to hours (12 h for complex $[(\eta^6\text{-bip})Ru(bpm)I]^+$ (**6**)) at 310 K. Density functional theory calculations on bpm complexes **1**–**6** suggest that aquation occurs *via* a more associative pathway in an $I_a \leftrightarrow I_d$ mechanistic continuum for which bond-making is of greater importance than bond-breaking. For both *p*-cym and bip bpm-containing complexes **1**–**6**, the calculated reaction barriers and overall reaction energies follow the order I > Br ≈ Cl which may explain the slow hydrolysis rate determined by UV-vis spectroscopy for iodido complexes **3** and **6**.

In general, we were not able to establish a correlation between hydrolysis rates and anticancer activity which implies that the mechanism of action for these series of complexes does not depend solely on this process. The half-sandwich Ru^{II} arene complexes containing phenanthroline (**11**) or bathophenanthroline (**13**) as *N,N′*-chelating ligands are more cytotoxic towards A2780 human ovarian cancer cells, in contrast to the analogous complexes containing bpm (**1**–**6**). X-ray crystal structures show that bip complexes (**4** and **6**) can form strong inter- and intra-ligand π-π interactions which enforces planarity on the bpm ligand, particularly in the case of complex **4**. An interesting feature of the structure of complex **7** is the presence of aromatic CH-*π* (bpm) interactions. Strong binding to 9-EtG, but not to 9-EtA, was observed for complexes containing *N,N′* chelating ligands such as bpm, phen and bathophen as well as different arenes such as *p*-cym, hmb, ind and thn. By the use of DFT calculations, the binding energies for model DNA nucleobases were

assessed. DFT calculations show that the 9-EtG nucleobase adducts of all complexes are thermodynamically preferred compared to their 9-EtA adducts by ca. 10 kcal mol^{-1}, explaining the guanine-specific binding observed experimentally for complexes **1**, **8**–**11** and **13**. DNA binding studies show that complexes **1** and **11** bind to DNA, suggesting that it could be target for these complexes, though the induced conformational changes are not significant. The reduced cytotoxic potency of the bpm-containing complexes might be due to the weakness of lesions on DNA or side reactions with other biomolecules such as glutathione (GSH). The formation of a presumably largely unreactive Ru^{II}-GS adduct might contribute to the lack of cytotoxicity [59].

Acknowledgements. S.B.-L. thanks WPRS/ORSAS (UK) and CONACyT (Mexico) for funding a research studentship. B. L., O. N. and V. B. were supported by the Czech Science Foundation (Grants P301/10/0598 and 301/09/H004).We also thank EDRF and AWM (Science City) and ERC (grant. no 247450) for funding, and Dr Ivan Prokes and Dr Lijiang Song and Mr. Philip Aston of the University of Warwick for their help with NMR and MS instruments, respectively.

Supporting Information Available.

Details of the preparation and characterization of all the complexes in this work. Crystallographic data for **3**, **4**, **6**, **7**, **14**; mass-to-charge ratios obtained from HR-MS spectra for the products of hydrolysis of Ru^{II} arene complexes **1**−**14**; mass-to-charge ratios obtained from HR-MS spectra for the products of interactions of Ru^{II} arene complexes **1**, **8**–**11**, and **13** with 9-EtG; changes in CD and LD spectra of CT-DNA modified by Ru^{II} arene complexes **1** and **11**; X-ray crystal structure of **4** showing a π-π stacking interaction; CH-π interaction in the crystal structure of 7; bis-water bridged interaction in the X-ray

crystal structure of **14**; ^{1}H-^{1}H NOESY NMR spectrum of **14** in D_2O (aromatic region only); time evolution of the hydrolysis reactions of complexes **1**–**13**; dependence of the absorbance during aquation of **1** at 310 K; ^{1}H NMR spectra recorded during a pH* titration of a solution of the aqua adduct of complex **1**; DFT-optimised geometry in the transition state [TS] during the hydrolysis reaction of the Ru^{II} arene cation **1**; ^{1}H NMR spectra of the reaction of **10** with 9-EtG in D_2O at 310 K after 510 min; optimised geometries for the guanine and adenine adducts; kinetics of the binding of complexes **1** and **11** to CT-DNA; hydrolysis reaction of complex **1** in the presence of 100-fold excess of GSH followed by UV-vis spectroscopy.

X-ray crystallographic data for complexes **3**, **6**, **14**, **4** and **7** are available as Supporting Information and have been deposited in the Cambridge Crystallographic Data Centre under the accession numbers CCDC 872981, 872982, 872983, 872984, 872985, respectively. Copies of the data can be obtained free of charge from the CCDC (12 Union Road, Cambridge CB2 1EZ, UK; tel: (+44) 1223-336-408; fax: (+44) 1223-336-003; e-mail: deposit@ccdc.cam.ac.uk; website link: (http://www.ccdc.cam.ac.uk/).

References

1. Jung Y, Lippard SJ (2007) Chem Rev 107:1387–1407.

2. van Zutphen S, Reedijk J (2005) Coord Chem Rev 249:2845–2853.

3. Pizarro AM, Habtemariam A, Sadler PJ (2010) Top Organomet Chem 32:21–56.

4. Aird RE, Cummings J, Ritchie AA, Muir M, Morris RE, Chen H, Sadler, PJ, Jodrell DI (2001) Br J Cancer 86:1652–1657.

5. Yan YK, Melchart M, Habtemariam A, Sadler PJ (2005) Chem. Commun 4764–4776.

6. (a) Fernández R, Melchart M, Habtemariam A, Parsons S, Sadler PJ (2004) Chem Eur J 10:5173–5179; (b) Wang F, Habtemariam A, van der Geer EPL, Fernández R, Melchart M, Deeth RJ, Aird R, Guichard S, Fabbiani FPA, Lozano-Casal P, Oswald IDH, Jodrell DI, Parsons S, Sadler PJ (2005) Proc Natl Acad Sci USA 102:18269–18274.

7. Bloemink MJ, Engelking H, Karentzopoulos S, Krebs B, Reedijk J (1996) Inorg Chem 35:619–627.

8. Nováková O, Kasparkova J, Vrana O, van Vliet PM, Reedijk J, Brabec V (1995) Biochemistry 34:12369–12378.

9. Velders AH, Kooijman H, Spek AL, Haasnoot JG, De Vos D, Reedijk J (2000) Inorg Chem 39:2966-2967.

10. (a) Ishikawa T, Ali-Osman F (1993) J Biol Chem 268:20116–20125; (b) Chen Y, Guo Z, Parkinson JA, Sadler PJ (1998) J Chem Soc Dalton Trans 3577–3585; (c) Teuben J.-M, Reedijk J (2000) J Biol Inorg Chem 5:463–468.

11. Corazza A, Harvey I, Sadler PJ (1996) Eur J Biochem 236:697−705.

12. Buttke TM, Sandstrom PA (1994) Immunol Today 15:7–10.

13. Clarke MJ (2002) Coord Chem Rev 232:69–93.

14. (a) Bennet MA, Smith AK (1974) J Chem Soc Dalton Trans 233–241; (b) Govindaswamy P, Canivet J, Therrien B, Süss-Fink G, Štěpnička P, Ludvík J (2007) J Organomet Chem 692:3664–3675; (c) Zelonka RA, Baird MC (1972) J Organomet Chem 35:C43–C46; (d) Melchart M, Habtemariam A, Nováková O, Moggach SA, Fabbiani FPA, Parsons S, Brabec V, Sadler PJ (2007) Inorg Chem 46:8950–8962.

15. Habtemariam A, Betanzos-Lara S, Sadler PJ (2010) Inorg Synth 35:160–163.

16. Brabec V, Palecek E (1970) Biophysik 6:290−300

17. Brabec V, Palecek E (1976) Biophys Chem 4:79−92.

18. Sheldrick GM SHELXL97, University of Göttingen, Germany, 1997.

19. (a) Sheldrick GM (1990) Acta Cryst A46:467−473; (b) Sheldrick GM (2008) Acta Cryst 64:12−122.

20. Krezel A, Bal W (2004) J Inorg Biochem 98:161–166.

21. (a) Te Velde G, Bickelhaupt FM, Baerends EJ, Fonseca Guerra C, Van Gisbergen SJA, Snijders JG, Ziegler T (2001) J Comp Chem 22:931–967; (b) Baerends EJ, Berces A, Bo C, Boerrigter PM, Cavallo L, Deng L, Dickson RM, Ellis DE, Fan L, Fischer TH *et. al.* (2000) ADF 2009 (Free University, Amsterdam).

22. (a) Wert C, Zener C (1949) Phys Rev 76:1169–1175; (b) Vineyard GH (1957) J Phys Chem Solids 3:121–127.

23. (a) Brabec V, Leng M (1993) Proc Natl Acad Sci USA 90:5345–5349; (b) Lemaire MA, Schwartz A, Rahmouni AR, Leng M (1991) Proc Natl Acad Sci USA 88:1982–1985.

24. Keck MV, Lippard SJ (1992) J Am Chem Soc 114:3386–3390.

25. Skehan P, Storeng R, Scudiero D, Monks A, McMahon J, Vistica D, Warren JT, Bokesch H, Kenney S, Boyd MR (1990) J Nat Cancer Inst 82:1107–1112.

26. (a) Morris RE, Aird RE, del Socorro Murdoch P, Chen H, Cummings J, Hughes ND, Parsons S, Parkin A, Boyd G, Jodrell DI, Sadler PJ (2001) J Med Chem 44:3616−3621; (b) Chen H, Parkinson JA, Parsons S, Coxall RA, Gould RO, Sadler PJ (2002) J Am Chem Soc 124:3064–3082.

27. (a) Süss-Fink G (2010) Dalton Trans 39:1673–1688; (b) Singh A, Chandra M, Sahay AN, Pandey DS, Pandey KK, Mobin SM, Puerta MC, Valerga P (2004) J Organomet Chem 689:1821–1834.

28. Flower KR, Pritchard RG (2001) J Organomet Chem 620:60–68.

29. Gül N, Nelson JH (1999) Organometallics 18:709–725.

30. Gül N, Nelson JH (1999) Polyhedron 18:1835–1843.

31. Bugarcic T, Habtemariam A, Stepankova J, Heringova P, Kašpárková J, Deeth RJ, Johnstone RDL, Prescimone A, Parkin A, Parsons S, Brabec V, Sadler PJ (2008) Inorg Chem 47:11470–11486.

32. (a) van Rijt SH, Hebden AJ, Amaresekera T, Deeth RJ, Clarkson GJ, Parsons S, McGowan P, Sadler PJ (2009) J Med Chem 52:7753–7764; (b) Bugarcic T, Nováková O,

Halámiková A, Zerzánková L, Vrána O, Kašpárková J, Habtemariam A, Parsons S, Sadler PJ, Brabec V (2008) J Med Chem 51:5310–5319.

33. Brandl M, Weiss MS, Jabs A, Suhnel J, Hilgenfeld R (2001) J Mol Biol 307:357–377.

34. Bogdanovic GA, Spasojevic-de Bire A, Zaric SD (2002) Eur J Inorg Chem 1599–1602.

35. (a) Dieter-Wurm I, Sabat M, Lippert B (1992) J Am Chem Soc 114:357–359; (b) Witkowshi H, Freisinger E, Lippert B (1997) J Chem Soc Chem Commun 1315–1316; (c) Sigel RKO, Freisinger E, Metzger S, Lippert B (1998) J Am Chem Soc 120:12000–12007.

36. Qu X, Chaires JB (2001) J Am Chem Soc 123:1–7.

37. Betanzos-Lara S, Salassa L, Habtemariam A, Sadler PJ (2009) Chem Commun 6622–6624.

38. Wang F, Chen H, Parsons S, Oswald IDH, Davidson JE, Sadler PJ (2003) Chem Eur J 9:5810–5820.

39. Kunkely H, Vogler A (2003) Inorg Chim Acta 343:357–360.

40. Dadci L, Elias H, Frey U, Hornig A, Koelle U, Merbach AE, Paulus H, Schneider JS (1995) Inorg Chem 34, 306–315.

41. Koefod RS, Mann KR (1990) J Am Chem Soc 112:7287–7293.

42. Dougan SJ, Melchart M, Habtemariam A, Parsons S, Sadler PJ (2007) Inorg Chem 46:10882–10894.

43. Rapaport I, Helm L, Merbach AE, Bernhard P, Ludi A (1988) Inorg Chem 27:873–879.

44. Broomhead JA, Basolo F, Pearson RG (1964) Inorg Chem 3:826–832.

45. Takeuchi KJ, Thompson MS, Pipes DW, Meyer TJ (1984) Inorg Chem 23:1845−1851.

46. (a) Basolo F, Pearson RG *Mechanisms of Inorganic Reactions: A Study of Metal Complexes in Solution*, Wiley, New York, 2nd Ed., 1967, p 124; (b) Broomhead JA, Kane-Maguire LAP (1968) Inorg Chem 7:2519–2523.

47. Scheller KH, Scheller-Krattiger V, Martin RB (1981) J Am Chem Soc 103:6833–6839.

48. Peacock AFA, Habtemariam A, Fernández R, Walland V, Fabbiani Francesca PA, Parsons S, Aird RE, Duncan IJ, Sadler PJ (2006) J Am Chem Soc 128:1739–1748.

49. Baik M-H, Friesner RA, Lippard SJ (2003) J Am Chem Soc 125:14082–14092.

50. Summa N, Schiessl W, Puchta R, van Eikema Hommes N, van Eldik R (2006) Inorg. Chem. 45: 2948–2959

51. Bancroft DP, Lepre CA, Lippard SJ (1990) J Am Chem Soc 112:6860–6871.

52. (a) Aird R, Cummings J, Ritchie A, Muir M, Morris R, Chen H, Sadler PJ, Jodrell D (2002) Br J Cancer 86:1652–1657; (b) Nováková O, Kasparkova J, Bursova V, Hofr C, Vojtiskova M, Chen H, Sadler PJ, Brabec V(2005) Chem Biol 12:121–129.

53. (a) Ivanov VI, Minchenkova LE, Minyat EE, Frank-Kamenetskii MD, Schyolkina AK (1974) J Mol Biol 87:817–833; (b) Vorlickova M (1995) Biophys J 69:2033–2043.

54. Keck MV, Lippard SJ (1992) J Am Chem Soc 114:3386–3390.

55. (a) Richards AD, Rodger A (2007) Chem Soc Rev 36:471−483; (b) Coggan DZM, Haworth IS, Bates PJ, Robinson A, Rodger A (1999) Inorg Chem 38:4486−4497; (c) Nováková O, Chen H, Vrana O, Rodger A, Sadler PJ, Brabec V (2003) Biochemistry

42:11544−11554; (d) Lincoln P, Broo A, Norden B (1996) J Am Chem Soc 118:2644−2653.

56. Habtemariam A, Melchart M, Fernández R, Parsons S, Oswald IDH, Parkin A, Fabbiani FPA, Davidson JE, Dawson A, Aird RE, Jodrell DI, Sadler PJ (2006) J Med Chem 49:6858–6868.

57. Liu HK, Berners-Price SJ, Wang FY, Parkinson JA, Xu JJ, Bella J, Sadler PJ (2006) Angew Chem Int Ed 45:8153–8156.

Tables

Table 1. Selected bond lengths (Å) and angles (°) for [(η^6-*p*-cym)Ru(bpm)I][PF_6] (**3**), [(η^6-bip)Ru(bpm)Cl][PF_6] (**4**), [(η^6-bip)Ru(bpm)I][PF_6] (**6**), [(η^6-etb)Ru(bpm)Cl][PF_6] (**7**), and [(η^6-*p*-cym)Ru(bpm)(9-EtG-*N7*)][PF_6]$_2$ (**14**).

Bond length/angle	**3**	**4**	**6**	**7**	**14**
Ru−arene$_{(centroid)}$	1.704	1.691	1.693	1.684	1.693
Ru(1)−I(1)	2.706(3)	–	2.70476(16)	–	–
Ru(1)−Cl(1)	–	2.402(8)	–	2.3743(9)	–
Ru(1)−N(13)	2.091(2)	–	–	–	2.1125(19)
Ru(1)−N(1)		2.092(2)	2.0901(12)	2.073(3)	2.0972(18)
Ru(1)−N(8)	2.0833(19)	2.093(2)	2.0833(12)	2.081(3)	2.0941(18)
C(6)−C(7)	1.472(4)	1.476(4)	1.477(2)	1.472(5)	1.477(3)
N(8)−Ru(1)−N(1)	76.78(8)	76.72(9)	76.90(5)	77.06(12)	77.05(7)
I(1)−Ru(1)−N(8)	86.38(6)	---	82.60(3)	–	–
Cl(1)−Ru(1)−N(8)	–	83.64(6)	–	83.36(8)	–
I(1)−Ru(1)−N(1)	85.79(6)	–	88.00(3)	–	–
Cl(1)−Ru(1)−N(1)	–	83.00(7)	–	84.67(8)	–
N(13)−Ru(1)−N(8)	–	–	–	–	86.59(7)
N(13)−Ru(1)−N(1)	–	–	–	–	88.64(7)

Table 2. Hydrolysis data for complexes **1**−**13** determined by UV-vis spectroscopy as 100 μM solutions (5% MeOH/95% H_2O) at 310 K.

	Compound	$t_{1/2}$ (min)	$k \times 10^{-3}$ (min^{-1})[a]
(**1**)	[(η^6-*p*-cym)Ru(bpm)Cl][PF_6]	92.3	7.51 ± 0.07
(**2**)	[(η^6-*p*-cym)Ru(bpm)Br][PF_6]	22.4	31.0 ± 0.91
(**3**)	[(η^6-*p*-cym)Ru(bpm)I][PF_6]	234.8	2.95 ± 0.08
(**4**)	[(η^6-bip)Ru(bpm)Cl][PF_6][b]	175.9	3.94 ± 0.04
(**5**)	[(η^6-bip)Ru(bpm)Br][PF_6][b]	39.7	17.0 ± 0.31
(**6**)	[(η^6-bip)Ru(bpm)I][PF_6][b]	714.6	0.97 ± 0.04
(**7**)	[(η^6-etb)Ru(bpm)Cl][PF_6][b]	14.5	50.0 ± 0.05
(**8**)	[(η^6-hmb)Ru(bpm)Cl][PF_6]	40.2	17.2 ± 1.32
(**9**)	[(η^6-ind)Ru(bpm)Cl][PF_6]	43.3	16.0 ± 0.15
(**10**)	[(η^6-thn)Ru(bpm)Cl][PF_6]	89.9	7.71 ± 0.44
(**11**)	[(η^6-*p*-cym)Ru(phen)Cl][PF_6]	22.8	30.5 ± 0.43
(**12**)	[(η^6-*p*-cym)Ru(phendio)Cl][PF_6][b]	59.6	11.6 ± 0.10
(**13**)	[(η^6-*p*-cym)Ru(bathophen)Cl][PF_6]	16.9	40.8 ± 0.86

[a] The errors are fitting errors

[b] The rate constants for complexes that underwent arene loss detected by ^{1}H NMR (**4**, **5**, **7**, and **12**) were determined over the period of time before the onset of arene loss.

Table 3. Equilibrium constants (K, μM) and percentage of arene loss of Ru^{II} arene complexes at equilibrium after 24 h of the hydrolysis reaction in a 100 μM (5% MeOD-d_4/95% D_2O) solution at 310 K of complexes **1**−**11** and **13** followed by ^1H NMR.

	Compound	K (μM)	% Arene loss
(**1**)	[(η^6-*p*-cym)Ru(bpm)Cl][PF_6]	280.5	0.0
(**2**)	[(η^6-*p*-cym)Ru(bpm)Br][PF_6]	790.6	0.0
(**3**)	[(η^6-*p*-cym)Ru(bpm)I][PF_6]	14.0	0.0
(**4**)	[(η^6-bip)Ru(bpm)Cl][PF_6]	9.0	48.1
(**5**)	[(η^6-bip)Ru(bpm)Br][PF_6]	10.4	68.3
(**6**)	[(η^6-bip)Ru(bpm)I][PF_6]	0.2	0.0
(**7**)	[(η^6-etb)Ru(bpm)Cl][PF_6]	4.5	2.9
(**8**)	[(η^6-hmb)Ru(bpm)Cl][PF_6]	34.1	0.0
(**9**)	[(η^6-ind)Ru(bpm)Cl][PF_6]	79.6	0.0
(**10**)	[(η^6-thn)Ru(bpm)Cl][PF_6]	231.1	0.0
(**11**)	[(η^6-*p*-cym)Ru(phen)Cl][PF_6]	61.6	0.0
(**13**)	[(η^6-*p*-cym)Ru(bathophen)Cl][PF_6]	52.1	0.0

Table 4. pK_a* values for the aqua adducts of complexes **1**, **8**,**9** and **11** at 298 K.

	Compound	pK_a
1	$[(\eta^6\text{-}p\text{-cym})Ru(bpm)OH_2]^{2+}$	6.96
8	$[(\eta^6\text{-hmb})Ru(bpm)OH_2]^{2+}$	7.04
9	$[(\eta^6\text{-ind})Ru(bpm)OH_2]^{2+}$	6.91
11	$[(\eta^6\text{-}p\text{-cym})Ru(phen)OH_2]^{2+}$	7.32

Table 5. Selected bond lengths, forward reaction barriers, and overall reaction energies from Density Functional Theory (DFT) calculations for the modeled reaction $\{[(\eta^6\text{-}p\text{-cym})Ru(bpm)X]^+ \cdot H_2O]\} \rightarrow [TS] \rightarrow \{[(\eta^6\text{-}p\text{-cym})Ru(bpm)OH_2]^{2+} \cdot Cl^-]\}$.

	Ru–X/Ru–OH_2 [RS] (Å)	Ru–X/Ru–OH_2 [TS] (Å)	Ru–X/Ru–OH_2 [P] (Å)	$\Delta E^{\ddagger}$ (kcal mol^{-1})	ΔE_{reacc} (kcal mol^{-1})
p-cym/bpm					
1 Cl	2.44736/3.87080	3.1069/2.67606	4.00637/2.17416	20.09	5.5
2 Br	2.58087/3.93448	3.29409/2.67608	4.13680/2.17987	21.01	7.28
3 I	2.76784/4.08973	3.58007/2.68230	4.42902/2.19029	22.79	9.61
bip/bpm					
4 Cl	2.43726/3.82308	3.01943/2.71710	4.01419/2.16185	19.96	6.16
5 Br	2.57062/3.88138	3.18568/2.73201	4.15467/2.16741	20.94	7.51
6 I	2.76183/4.01231	3.45171/2.74296	4.41027/2.17431	22.28	10.28

[RS] = Resting state
[TS] = Transition state
[P] = Product
ΔE_{reacc} values relative to reactant species at zero

Table 6. Solution (COSMO) 9-EtG and 9-EtA binding energies for adducts of Ru^{II} arene complexes **1**, **8**–**11** and **13**.

Compound	9-EtG (kcal mol^{-1})	9-EtA (kcal mol^{-1})
1	38.5	30.8
8	39.3	30.3
9	39.3	32.4
10	41.0	34.4
11	39.8	33.7
13	38.7	32.3

Table 7. Percentage binding of complexes **1** and **11** to CT-DNA (1.0×10^{-4} M) in 10 mM $NaClO_4$ at 310 K as determined by FAAS after 24 h.

	% Ru^{II} bound	
Method	(**1**)[a]	(**11**)[a]
DNA precipitation by EtOH	61.0	62.0
Dialysis against 10 mM $NaClO_4$	77.0	19.6
Dialysis against 0.1 M NaCl	21.6	17.3

[a] Data are the average of two independent experiments

Table 8. Unwinding of supercoiled pUC19 DNA by Ru^{II} arene complexes [(η^6-*p*-cym)Ru(bpm)Cl][PF_6] (**1**) and [(η^6-*p*-cym)Ru(phen)Cl][PF_6] (**11**).

Compound		r_b(c)	Unwinding Angle (°)
(**1**)	[(η^6-*p*-cym)Ru(bpm)Cl][PF_6]	0.13	7.7±1.7
(**11**)	[(η^6-*p*-cym)Ru(phen)Cl][PF_6]	0.15	6.6±1.7
Cisplatin		0.08	13.0±0.4

Table 9. IC_{50} values for Ru^{II} arene complexes **11** and **13** against the A2780 human ovarian cancer cell line.

	Compound	IC_{50} μM (A2780)[a]
(**11**)	[(η^6-*p*-cym)Ru(phen)Cl][PF_6]	22.9
(**13**)	[(η^6-*p*-cym)Ru(bathophen)Cl][PF_6]	0.5
	Cisplatin	1.1

[a] Complexes **1**−**6**, and **8**−**10** had IC_{50} values larger than 100 μM against the cell lines tested (cisplatin 1.0 μM under the same conditions)

Figures Caption

Figure 1. General structures of the complexes studied in this work, synthesized as PF_6 salts.

Figure 2. X-ray structure of the cations in [(η^6-*p*-cym)Ru(bpm)I][PF_6] (**3**), [(η^6-bip)Ru(bpm)Cl][PF_6] (**4**), [(η^6-bip)Ru(bpm)I][PF_6]$_2$ (**6**), [(η^6-etb)Ru(bpm)Cl][PF_6] (7), and [(η^6-*p*-cym)Ru(9-EtG-*N7*)][PF_6]$_2$ (**14**). Thermal ellipsoids show 50% probability. The hydrogen atoms and counter ions have been omitted for clarity.

Figure 3. Hydrolysis reaction modeled for the Ru^{II} arene cations [(η^6-arene)Ru(bpm)X]$^+$ of complexes **1**–**6**. [TS] is transition state.

Figure 4. DFT-optimised geometry of the transition state [TS] during the hydrolysis reaction of the Ru^{II} arene cation [(η^6-*p*-cym)Ru(bpm)Cl]$^+$ (**1**).

Figure 5. Time dependence of the ^{1}H NMR spectra of a 100 μM solution of [(η^6-*p*-cym)Ru(phen)Cl][PF_6] (**11**) in D_2O at 310 K in the presence of an equimolar amount of 9-EtG. Blue = [(η^6-*p*-cym)Ru(phen)Cl]$^+$, Green =[(η^6-*p*-cym)Ru(phen)(OH_2)]$^{2+}$, Magenta = [(η^6-*p*-cym)Ru(phen)(9-EtG-*N7*)]$^{2+}$; ★ = phen, ● = *p*-cym; ♦ = bound 9-EtG-*N7*.

Figure 6. Numbering scheme for the nucleobases 9-EtG and 9-EtA.

Figure 7. Autoradiogram of 6% polyacrylamide/8 M urea sequencing gel showing inhibition of RNA synthesis by T7 RNA polymerase on the *Nde*I/*Hpa*I fragment containing adducts of Ru^{II} arene complexes and cisplatin. Lanes: control, unmodified template; A, U, G and C, chain terminated marker DNAs; cisplatin, **1** and **11**, the template modified by cisplatin at $r_b = 0.02$, Ru^{II} arene complexes **1** at $r_b = 0.02$ or **11** at $r_b = 0.015$, respectively.

Figure 8. Schematic diagram showing the portion of the sequence used to monitor inhibition of RNA synthesis by Ru^{II} arene complexes. The arrow indicates the start of the T7 RNA polymerase, which used as template the bottom strand of the *Nde*I/*Hpa*I fragment of pSP73KB. The closed bullets represent major stop sites for DNA modified by complex **1** or **11**, respectively. The numbers correspond to the nucleotide numbering in the sequence map of the pSP73KB plasmid.

Figure 9. The unwinding of supercoiled pUC19 plasmid DNA by complexes **1** (top) and **11** (bottom). The plasmid was incubated with Ru^{II} arene complexes in 10 mM $NaClO_4$, at pH 6 for 24 h at 310 K. Lanes in the top panel: **1** and **10**, control, unmodified DNA; 2, $r_b = 0.06$; 3, $r_b = 0.08$; 4, $r_b = 0.09$; 5, $r_b = 0.12$; 6, $r_b = 0.14$; 7, $r_b = 0.16$; 8, $r_b = 0.18$; 9, $r_b = 0.20$. Lanes in the bottom panel: 1 and 10, control, unmodified DNA; 2, $r_b = 0.05$; 3, $r_b = 0.06$; 4, $r_b = 0.07$; 5, $r_b = 0.08$; 6, $r_b = 0.09$; 7, $r_b = 0.11$; 8, $r_b = 0.13$; 9, $r_b = 0.15$. The top bands in

each panel correspond to the form of nicked plasmid and the bottom bands to the closed, negatively supercoiled plasmid.

Figure 10. Circular dichroism spectra of CT-DNA modified by Ru^{II} arene complexes **1** and **11**. CD spectra were recorded for DNA in 10 mM $NaClO_4$. The concentration of DNA was 3.3×10^{-4} M. The values of r_b were in the range of 0.013−0.047.

Figure 11. Linear dichroism spectra of CT-DNA modified by Ru^{II} arene complexes **1** (top) and **11** (bottom). LD spectra were recorded for DNA in 10 mM $NaClO_4$. The concentration of DNA was 3.3×10^{-4} M. The values of r_b were in the range of 0.013−0.047.

Figure 12. ^{1}H NMR spectra of the reaction of a 100 μM solution of [(η^6-*p*-cym)Ru(bpm)Cl][PF_6] (**2**) with 100-fold excess of GSH in D_2O at 310 K after 24 h. Blue = [(η^6-*p*-cym)Ru(bpm)Cl]$^+$; Green = [(η^6-*p*-cym)Ru(bpm)OH_2]$^{2+}$; Yellow = [(η^6-*p*-cym)Ru(bpm)(G*S*H)]$^+$;■ = bpm, ● = *p*-cym.

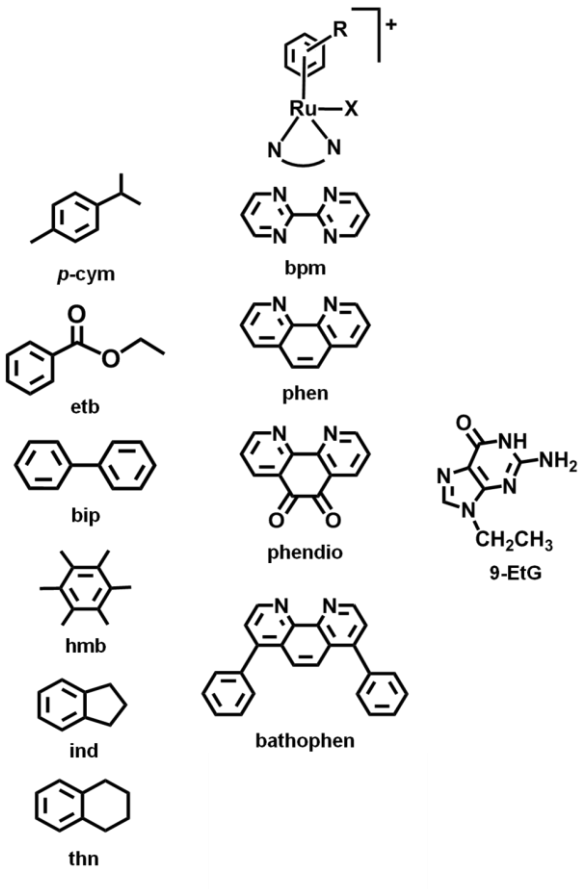

Compound	Arene	N,N' / N,S	X
1	*p*-cym	bpm	Cl
2	*p*-cym	bpm	Br
3	*p*-cym	bpm	I
4	bip	bpm	Cl
5	bip	bpm	Br
6	bip	bpm	I
7	etb	bpm	Cl
8	hmb	bpm	Cl
9	ind	bpm	Cl
10	thn	bpm	Cl
11	*p*-cym	phen	Cl
12	*p*-cym	phendio	Cl
13	*p*-cym	bathophen	Cl
14	*p*-cym	bpm	9-EtG

Figure 1.

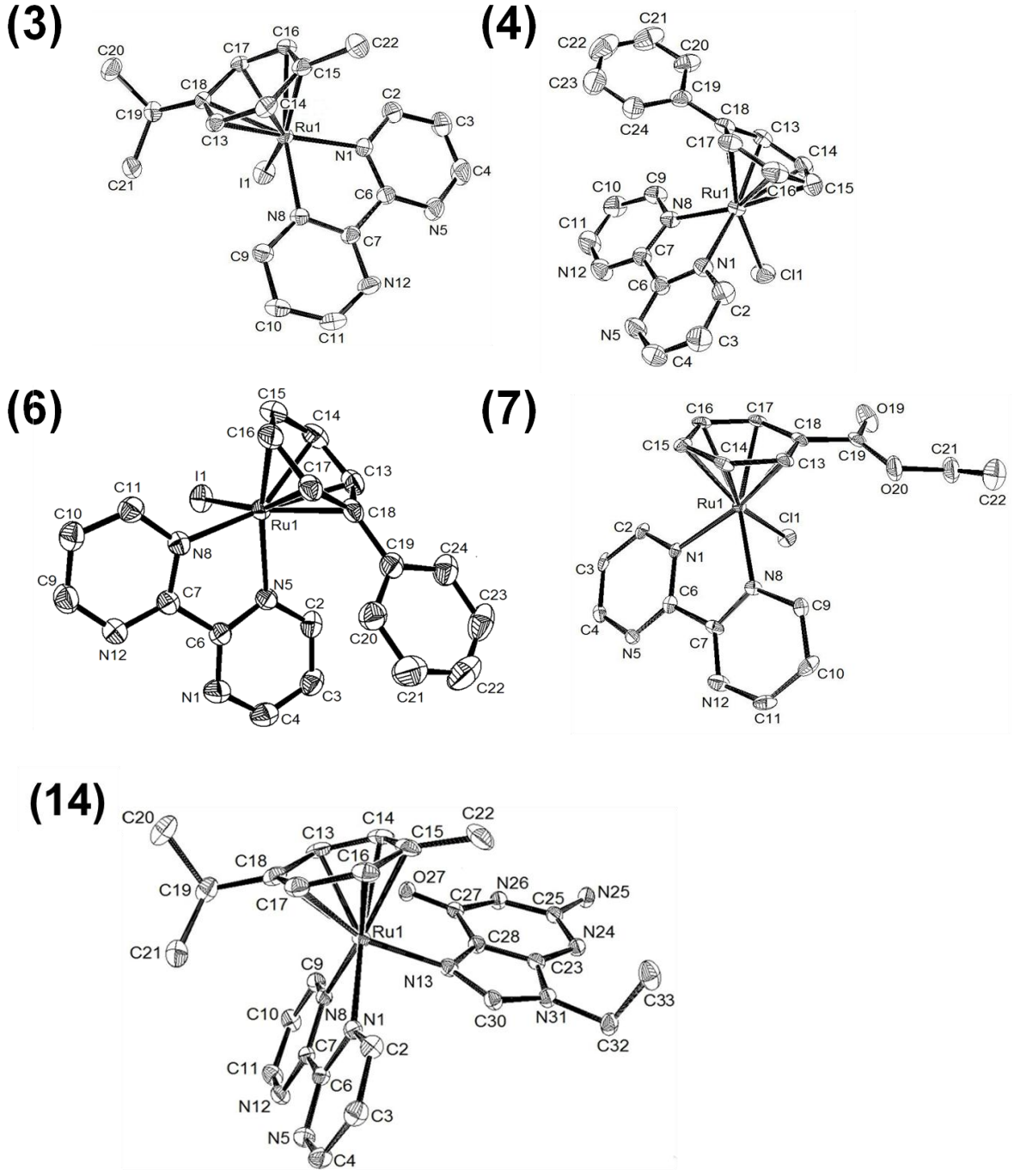
(3)
C20
C17
C16
C22
C15
C18
C14
C2
C19
Ru1
C3
C13
N1
C4
I1
C21
C6
N8
N5
C7
C9
N12
C10
C11
(4)
C21
C22
C20
C23
C19
C18
C24
C13
C17
C14
C10
C9
Ru1
C16
C15
N8
C11
C7
N12
N1
Cl1
C6
C2
N5
C3
C4
(6)
C15
C14
C16
C17
C13
I1
C11
C18
C10
Ru1
N8
C19
C24
C9
C7
N5
C2
C23
C20
C6
N12
N1
C3
C21
C22
C4
(7)
C16
C17
O19
C18
C15
C14
C13
C19
C21
O20
C22
Ru1
Cl1
C2
N1
C3
N8
C6
C9
C4
N5
C7
C10
N12
C11
(14)
C20
C14
C22
C13
C15
C18
C16
O27
N26
C19
C27
C25
N25
C17
Ru1
C28
N24
C21
C23
C9
N13
C33
C10
N8
N1
C30
N31
C32
C7
C2
C11
C6
N12
C3
N5
C4

Figure 2.

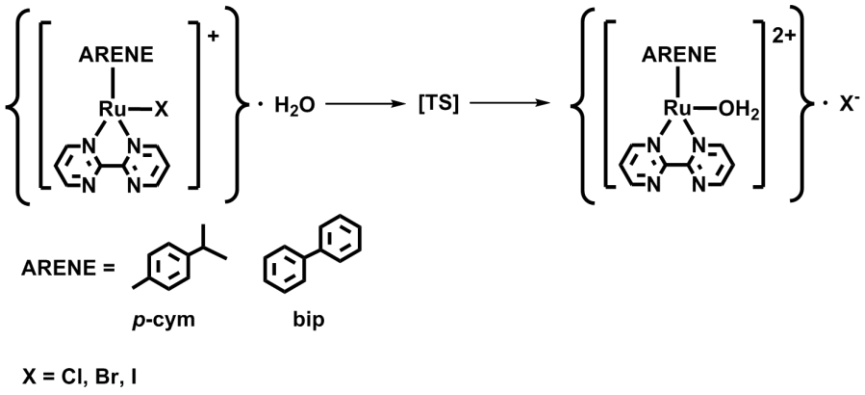

Figure3.

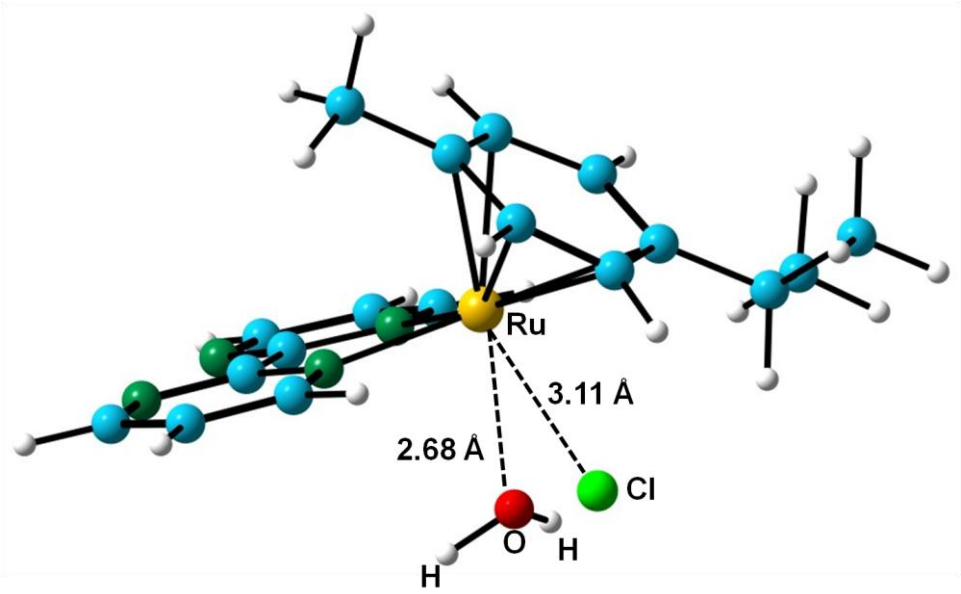

Figure 4.

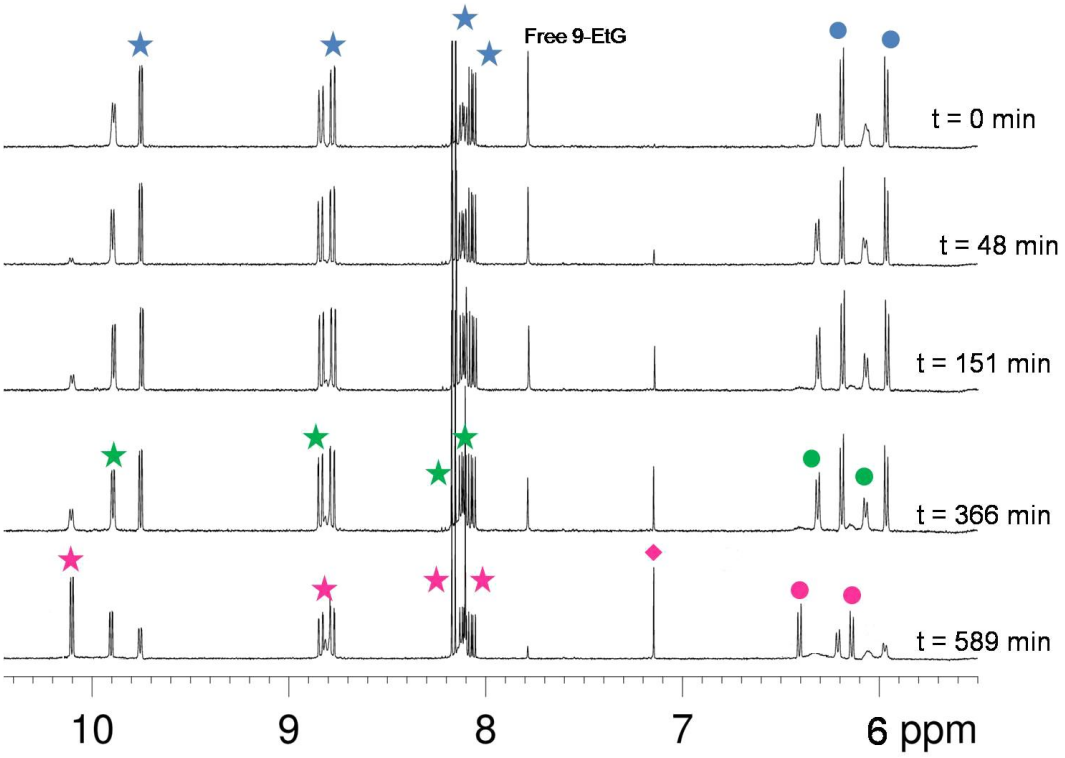

Figure 5.

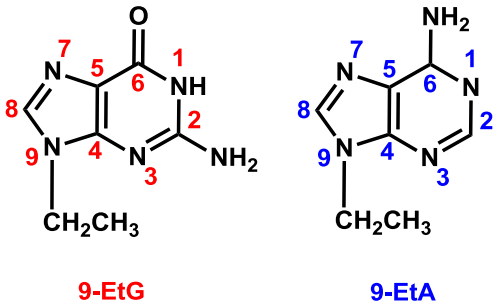
O
7
5
1
6
NH
8
2
9
4
N
3
NH2
CH2CH3
9-EtG
NH2
7
5
1
6
N
8
2
9
4
N
3
CH2CH3
9-EtA

Figure 6.

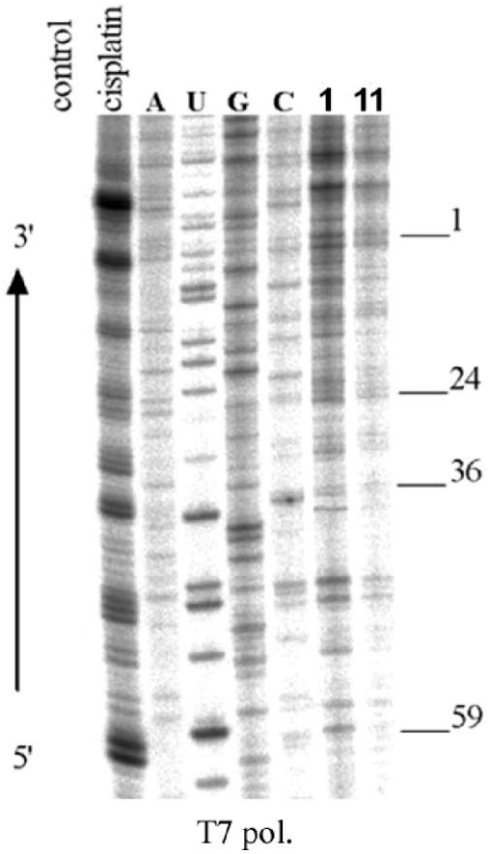
control
cisplatin
A
U
G
C
1
11
3'
5'
1
24
36
59
T7 pol.

Figure 7.

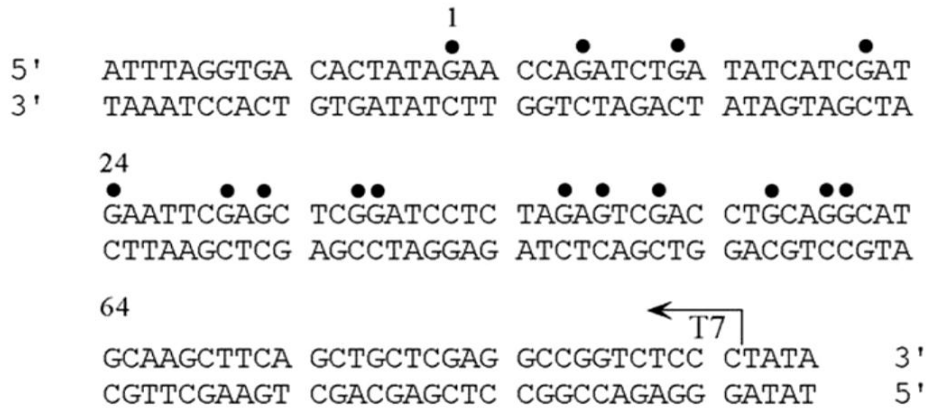

Figure 8.

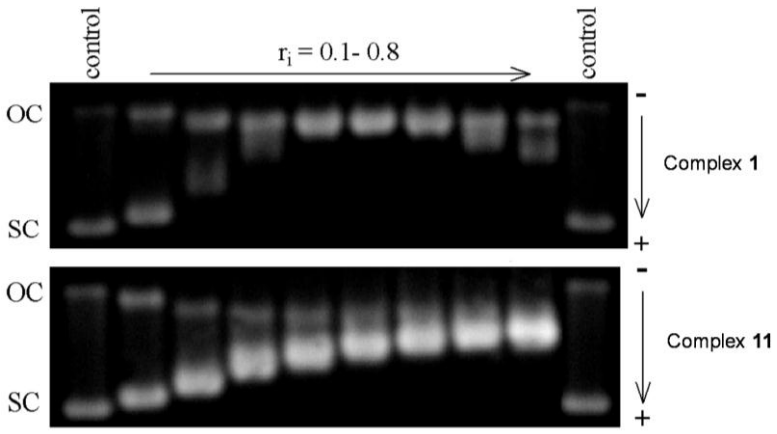

Figure 9.

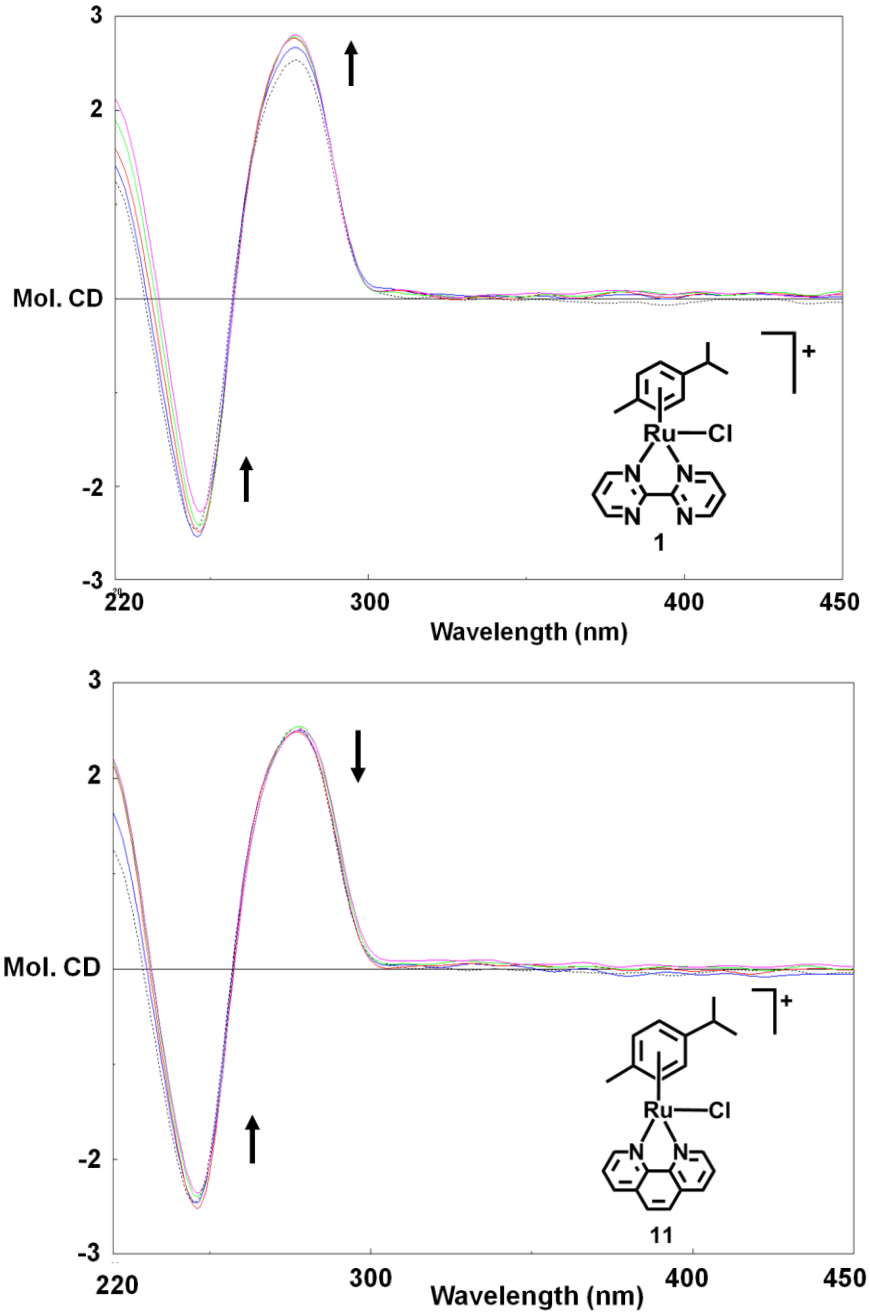
3
2
Mol. CD
-2
-3
220
300
400
450
Wavelength (nm)
Ru—Cl
N
N
N
N
+
1
3
2
Mol. CD
-2
-3
220
300
400
450
Wavelength (nm)
Ru—Cl
N
N
+
11

Figure 10.

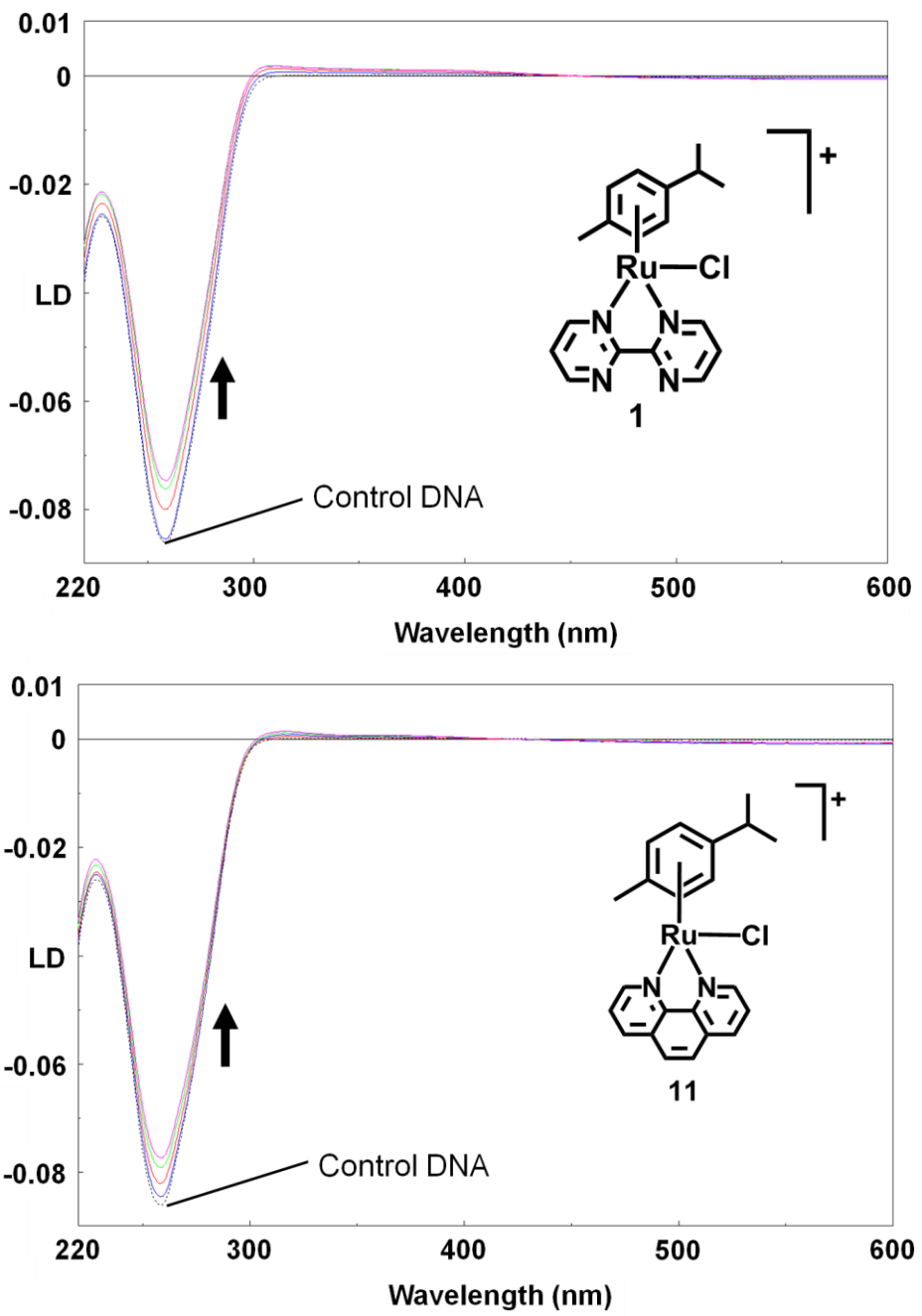
0.01
0
-0.02
LD
-0.06
-0.08
220
300
400
500
600
Wavelength (nm)
Control DNA
Ru—Cl
N
N
N
N
+
1
0.01
0
-0.02
LD
-0.06
-0.08
220
300
400
500
600
Wavelength (nm)
Control DNA
Ru—Cl
N
N
+
11

Figure 11.

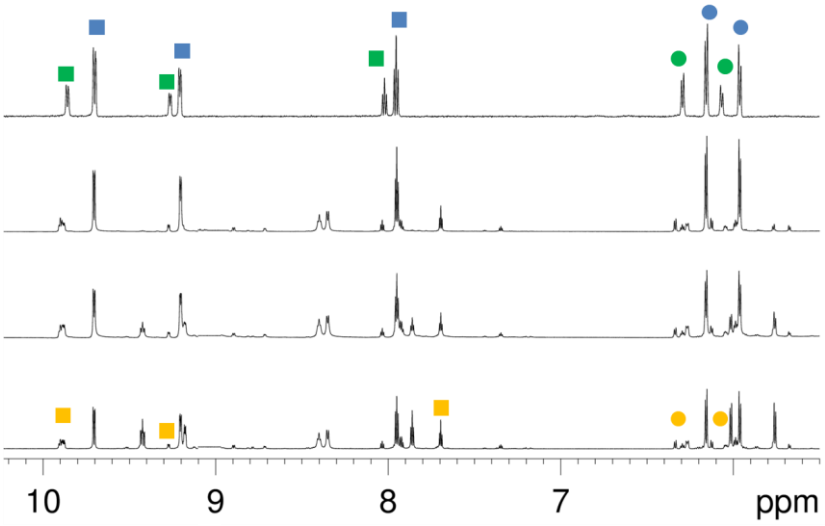

Figure 12.

****